



**HAL**  
open science

# The north cycladic detachment system and associated mineralization, Mykonos, Greece: Insights on the evolution of the Aegean domain

Armel Menant, Laurent Jolivet, Romain Augier, Nikolaos Skarpelis

## ► To cite this version:

Armel Menant, Laurent Jolivet, Romain Augier, Nikolaos Skarpelis. The north cycladic detachment system and associated mineralization, Mykonos, Greece: Insights on the evolution of the Aegean domain. *Tectonics*, 2013, 32, pp.433-452. 10.1002/tect.20037 . insu-00819811

**HAL Id: insu-00819811**

**<https://insu.hal.science/insu-00819811>**

Submitted on 20 Feb 2014

**HAL** is a multi-disciplinary open access archive for the deposit and dissemination of scientific research documents, whether they are published or not. The documents may come from teaching and research institutions in France or abroad, or from public or private research centers.

L'archive ouverte pluridisciplinaire **HAL**, est destinée au dépôt et à la diffusion de documents scientifiques de niveau recherche, publiés ou non, émanant des établissements d'enseignement et de recherche français ou étrangers, des laboratoires publics ou privés.

# The North Cycladic Detachment System and associated mineralization, Mykonos, Greece: Insights on the evolution of the Aegean domain

Armel Menant,<sup>1,2,3</sup> Laurent Jolivet,<sup>1,2,3</sup> Romain Augier,<sup>1,2,3</sup> and Nikolaos Skarpelis<sup>4</sup>

Received 2 May 2012; revised 2 March 2013; accepted 15 March 2013; published 30 May 2013.

[1] In the Aegean back-arc domain, some 30–35 Ma ago, an increase of the rate of slab retreat led to the initiation of post-orogenic extension, largely accommodated by large-scale structures such as the North Cycladic Detachment System (NCDS). Although this extension is still active nowadays, an E–W compressional regime developed in the Late Miocene with the propagation of the North Anatolian Fault. On Mykonos island (Cyclades), the NE–SW back-arc extension is particularly well expressed with the Livada and Mykonos detachments that belong to the NCDS and that are associated with NW–SE barite veins emplaced during the synkinematic cooling of the Mykonos intrusion. This study shows that the formation of the mineralization occurred when the pluton crossed the ductile-to-brittle transition during its exhumation below the NCDS at ~11–10 Ma. In addition, the kinematics of mineralized structures evolved with time: (1) most of the displacement was accommodated by the top-to-the-NE Livada and Mykonos detachments accompanied by the formation of mineralized normal faults that were (2) reworked in a strike-slip regime with an E–W direction of shortening and a persistent NE–SW stretching and (3) a late post-mineralization E–W compressional stage with a minor reworking of shallow-dipping faults (locally including the detachments themselves). We interpret this increase of the E–W shortening component recorded during the mineral deposition as a consequence of the initiation of the westward motion of Anatolia from 10 Ma, thus 4 Ma before the propagation of the North Anatolian Fault in the Dardanelles Strait and the localization of the strain on the Aegean Sea margins.

**Citation:** Menant, A., L. Jolivet, R. Augier, and N. Skarpelis (2013), The North Cycladic Detachment System and associated mineralization, Mykonos, Greece: Insights on the evolution of the Aegean domain, *Tectonics*, 32, 433–452, doi:10.1002/tect.20037.

## 1.. Introduction

[2] The Aegean domain in the eastern Mediterranean results from the Tertiary subduction of the African plate below Eurasia. Since the late Cretaceous–Paleocene closure of the Vardar Ocean, continuing convergence has led to the formation of the Hellenic orogenic wedge. Some 35 Ma ago, an increasing rate of slab retreat favored the formation of the Aegean Sea back-arc basin while shortening continued in peripheral areas [Le Pichon and Angelier, 1979; Jolivet and Faccenna, 2000]. This pervasive NE–SW to N–S Oligocene–Miocene extension was mainly accommodated by a limited number of low-angle normal faults or

detachments that controlled the exhumation of a series of metamorphic core complexes (MCCs) [Lister *et al.*, 1984; Gautier and Brun, 1994a; 1994b; Jolivet *et al.*, 1994; Ring *et al.*, 2010; Grasemann *et al.*, 2012]. In the northern part of Cyclades, this set of detachments is known as the North Cycladic Detachment System (NCDS) that accommodated several tens of kilometers of displacement [Jolivet *et al.*, 2010]. Further south, the West Cycladic Detachment System also participated in the exhumation of the metamorphic rocks [Grasemann *et al.*, 2012]. More recently, the Anatolian plate started its fast westward movement, revealed especially by Global Positioning System (GPS) and satellite laser ranging data [Reilinger *et al.*, 1997; 2010], partly as a consequence of the collision between Eurasia and Arabia [Armijo *et al.*, 1996; 1999] and partly as the result of detachments and tears of the African slab in the upper mantle [de Boorder *et al.*, 1998; Govers and Wortel, 2005; Faccenna *et al.*, 2006; Royden and Papanikolaou, 2011]. This plate motion is accommodated in particular by a large intracontinental discontinuity: the dextral strike-slip North Anatolian Fault (NAF) that induced the progressive localization of strain in the Aegean region, notably along the Central Hellenic Shear Zone (CHSZ) [Armijo *et al.*, 1996; Royden and Papanikolaou, 2011]. The

<sup>1</sup>Université d'Orléans, ISTO, Orléans, France.

<sup>2</sup>CNRS/INSU, ISTO, Orléans, France.

<sup>3</sup>BRGM, ISTO, Orléans, France.

<sup>4</sup>Faculty of Geology and Geoenvironment, University of Athens, Department of Economic Geology and Geochemistry, Athens, Greece.

Corresponding author: A. Menant, Université d'Orléans, ISTO, UMR 7327, 45071, Orléans, France. (armel.menant@cnrs-orleans.fr)

©2013. American Geophysical Union. All Rights Reserved.  
0278-7407/13/10.1002/tect.20037

NAF entered the Aegean domain through the Dardanelles Strait at ~6–5 Ma [Armijo *et al.*, 1999; Melinte-Dobrinescu *et al.*, 2009]. However, several studies in Anatolia have suggested that the present-day NAF results from the evolution of a wider dextral shear zone that dates back to the middle Miocene [Sengör *et al.*, 2005]. A number of additional observations such as open folds, strike-slip faults, and minor thrusts in the central Aegean domain and in western Turkey suggest, despite the strong back-arc N–S stretching, a significant component of E–W shortening [Angelier, 1976; Buick, 1991a; 1991b; Bozkurt and Park, 1997; Ring *et al.*, 1999; Avigad *et al.*, 2001; Bozkurt, 2003]. This compressional regime could be a consequence of the extrusion of Anatolia [Avigad *et al.*, 2001] that would have affected this region before the localization of strain on the edges of the Aegean Sea. The accurate timing for the initiation of this E–W shortening is however not well constrained. A closer look at the tectonic evolution of the central Aegean during the late Miocene allows us to describe more precisely the strain regime change.

[3] On Mykonos island (northern Cyclades), where extensional structures related to the activity of the NCDS have been described in details [Faure and Bonneau, 1988; Lee and Lister, 1992; Lucas, 1999; Lecomte *et al.*, 2010; Denèle *et al.*, 2011], a syntectonic granitoid intruded the Cycladic basement during the Serravallian and early Tortonian. Radiometric time constraint yielded a  $13.5 \pm 0.3$  Ma U–Pb crystallization age on zircon and  $11.5 \pm 0.5$  Ma to  $8.9 \pm 0.4$  Ma (U–Th)/He final cooling ages on apatite [Brichau *et al.*, 2008], at the time of the possible initiation of the westward movement of Anatolia. On the eastern part of the island, two branches of the NCDS have been recognized: the lower ductile-brittle Livada detachment and the upper brittle Mykonos detachment [Lecomte *et al.*, 2010]. Located in the vicinity of these structures, numerous mineralized occurrences, mainly barite veins belonging to the Aegean Cenozoic metallogenic province, have been described [Skarpelis, 2002]. The orientation of these veins clearly shows a conspicuous relation with the Aegean extensional tectonics [Lecomte *et al.*, 2010]. However, detailed geological mapping of the detachments and barite veins as well as detailed observations of the interrelations between strain and veins formation remain still poorly investigated.

[4] Based on field observations, this paper aims at understanding the relationships between mineralization and deformation on Mykonos island. Moreover, recognition of the successive tectonic regimes prior, during, and after mineral deposition has new implications for late Cenozoic geodynamic evolution of the Aegean domain.

## 2. Geological and Geodynamic Setting

### 2.1. Late Cenozoic Geodynamic Evolution of the Aegean Domain

[5] In the Mediterranean realm, the collision between the African and Eurasian plates during the Cenozoic led to the formation of several orogenic belts, including the Hellenides formed by accretion of both oceanic and continental units [Dercourt *et al.*, 1986; 1993; Stampfli, 2000; van Hinsbergen *et al.*, 2005]. Within the orogenic wedge, buried units (e.g., the Cycladic Blueschists) were affected by an initial high-pressure and low-temperature metamorphism (HP–LT) and were partly exhumed in a synorogenic context [Bonneau and Kienast,

1982; Trotet *et al.*, 2001]. Then, the subduction front started to migrate southward some 35 Ma ago with the collapse of the central part of the Hellenic belt, in direct response to slab retreat. Metamorphic rocks were thus transferred in the back-arc domain where they were exhumed in a post-orogenic extensional context [Jolivet and Faccenna, 2000; Jolivet and Brun, 2010]. The exact timing of the initiation of the slab retreat and the coeval inception of extension in the upper plate is however still debated and possibly as young as 25 Ma [Ring *et al.*, 2010].

[6] In the Cyclades, the HP–LT Cycladic Blueschists, belonging to the Pindos oceanic domain, reached their peak-pressure during the formation of the Hellenides some 50–45 Ma ago [Wijbrans and McDougall, 1986; 1988] and were exhumed during the Eocene as an extrusion wedge within the subduction channel [Jolivet *et al.*, 2003; Ring *et al.*, 2007; 2010; Brun and Faccenna, 2008; Huét *et al.*, 2009; Jolivet and Brun, 2010]. They are particularly well preserved in Syros and Sifnos islands where synorogenic shear zones are also well exposed [Trotet *et al.*, 2001; Keiter *et al.*, 2004; Philippon *et al.*, 2011]. After 35 Ma, post-orogenic extension started in the Cyclades, due to an increased rate of southward African slab roll-back that induced a delamination of the lower crust and mantle of the upper plate. Therefore, a warmer regime developed in the back-arc region leading to the formation of low-pressure and high-temperature (LP–HT) mineral assemblages which partly overprinted the former HP–LT parageneses of the Cycladic Blueschists (e.g., Andros, Tinos, and Naxos islands) and the underlying Cycladic basement (e.g., Ios and Sikinos islands). These LP–HT units were exhumed as metamorphic core complexes (MCC) between 35 and 8 Ma from the North to the South of the Cyclades [Lister *et al.*, 1984; Gautier and Brun, 1994a; 1994b; Vanderhaeghe, 2004; Brichau *et al.*, 2006; 2007; 2008; 2010; Duchêne *et al.*, 2006; Martin *et al.*, 2006].

[7] The exhumation, whether along HP–LT or HT–LP path, is controlled by crustal scale ductile-to-brittle extensional shear zones separating the Cycladic Blueschists in the footwall from the low-grade Upper Cycladic Unit in the hanging wall. In the northern Cyclades, this tectonic contact corresponds to the NCDS that crops out on the islands of Andros, Tinos, Mykonos, and Ikaria (Figure 1a) and shows a consistent top-to-the-NE sense of shear [Faure *et al.*, 1991; Lee and Lister, 1992; Gautier and Brun, 1994a; Ring and Layer, 2003; Kumerics *et al.*, 2005; Mehl *et al.*, 2005; Brichau *et al.*, 2007; 2008; Jolivet *et al.*, 2010; Lecomte *et al.*, 2010]. Syntectonic sediments, related to the activity of the NCDS, were deposited within fault-bounded basins from early (?) to late Miocene on Mykonos island [Sánchez-Gómez *et al.*, 2002]. Some 17 Ma ago, back-arc magmatism appeared in the Cyclades leading to the emplacement at mid-crustal levels of several syn-extensional intrusions formed by magmas involving both a mantle-derived mafic component and a voluminous crustal felsic component (e.g., Tinos, Delos, Mykonos, Ikaria, Serifos, and Naxos) [Altherr *et al.*, 1982; Faure *et al.*, 1991; Altherr and Siebel, 2002; Pe-Piper and Piper, 2002; 2006; Denèle *et al.*, 2011]. Finally, the westward extrusion of Anatolia started, adding an ~E–W shortening to the overall N–S extension of the Aegean domain [Avigad *et al.*, 2001]. This motion was then progressively accommodated by the NAF which propagated in the Dardanelles Strait and the North Aegean Trough some 6–5 Ma ago and joined the Evia and Corinth rifts, forming the CHSZ where the deformation is still concentrated nowadays

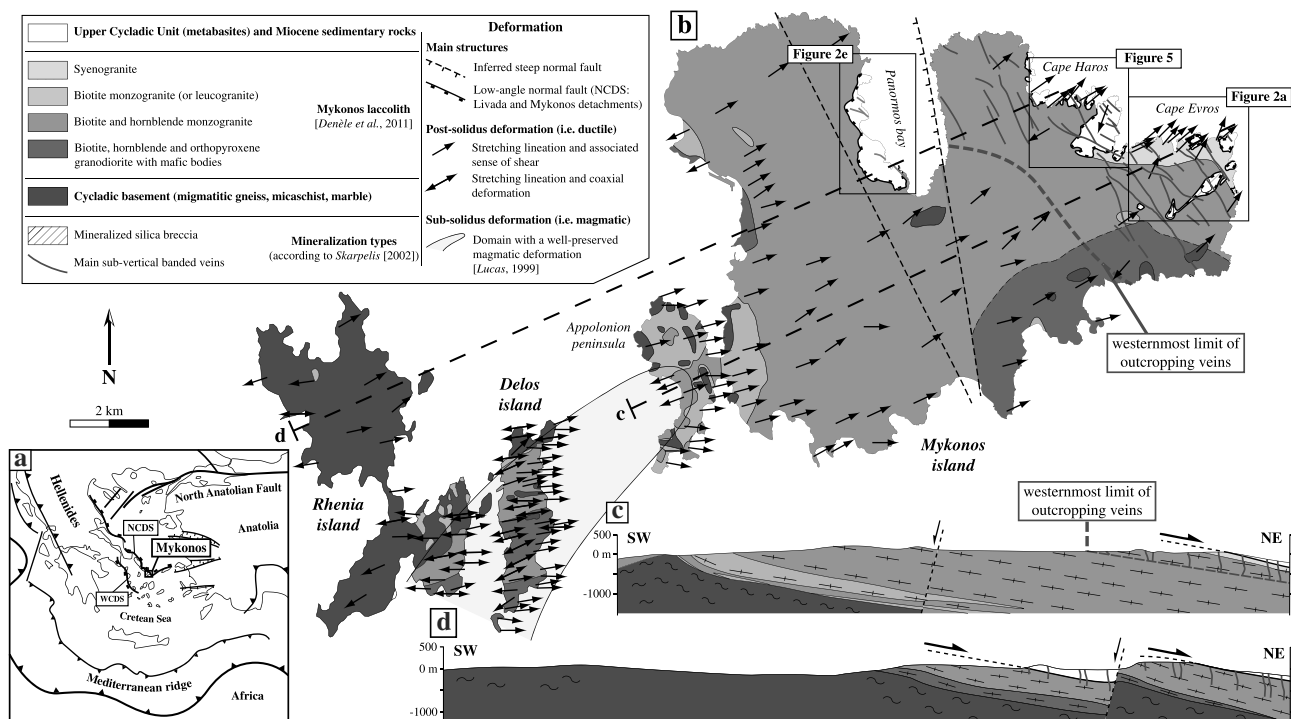


**Figure 1.** Tectonic and geological maps and location of the study area. (a) Simplified tectonic map of the Aegean domain, given is the location of Mykonos island. (b) Geological map of Mykonos island. (c and d) Cross-sections of Mykonos island oriented parallel to the stretching direction (modified from *Lucas* [1999]; *Lecomte et al.* [2010]; *Denèle et al.* [2011]). The westernmost limit of outcropping veins is reported on the (Figure 1b) geological map and the (Figure 1c) cross-section in order to estimate the current maximal depth of veins.

and generates a significant seismicity [*Armijo et al.*, 1996; *Le Pichon and Kreemer*, 2010; *Royden and Papanikolaou*, 2011].

## 2.2. Geological and Metallogenic Overview of Mykonos Island

[8] Mykonos island is mainly constituted by an I-type granitoid interpreted as an asymmetrical laccolith-like intrusion with a  $N70^{\circ}E$  long axis [*Denèle et al.*, 2011] whose fast cooling from  $\sim 680$  to  $\sim 60^{\circ}C$  occurred between 13 and 9 Ma [*Brichau et al.*, 2008]. This laccolith complex intrudes an extensional migmatitic dome, mainly constituted by paragneisses that belongs to the Cycladic basement cropping out on the Apollonion peninsula and on the neighboring Delos and Rhenia islands (Figure 1) [*Lucas*, 1999; *Pe-Piper et al.*, 2002; *Denèle et al.*, 2011]. The composition of the Mykonos laccolith evolves from a monzogranite to a granodiorite with an inverted zonation (i.e., more mafic toward the pluton center) [*Lucas*, 1999], which indicates a polyphased emplacement by successive pulses of magma injection. The dominant source of this magma corresponds to partial melting of biotite gneiss metasedimentary protolith similar to the metagreywackes of Rhenia island [*Stouraiti et al.*, 2010]. The laccolith displays primarily an intense magmatic fabric over which a protomylonitic to mylonitic deformation is superimposed and intensifies toward the two branches of the NCDS observed on the island (i.e., the Livada and Mykonos detachments; Figure 1c) [*Lucas*, 1999; *Jolivet et al.*, 2010; *Denèle et al.*, 2011]. The stretching lineations draw a curved pattern from  $\sim N90^{\circ}E$  in the Apollonion peninsula toward a

more northerly direction ( $N30-20^{\circ}E$ ) close to the NCDS with conspicuous top-to-the-NE kinematic indicators (Figure 1b). With a stretching lineation trending between  $N90^{\circ}E$  and  $N60^{\circ}E$  in most of the island, Mykonos contrasts with other Cycladic islands where the lineation is dominantly  $N30-20^{\circ}E$  [*Gautier and Brun*, 1994a; 1994b; *Jolivet et al.*, 1994]. *Denèle et al.* [2011] ascribe this curvature of lineation to differential block rotation during exhumation of the laccolith and its progressive cooling while the regional direction of extension remained constant about  $N20^{\circ}E$  [*Walcott and White*, 1998; *Jolivet*, 2001].

[9] The Livada detachment mostly exhibits a top-to-the-NE ductile deformation, locally evolving to brittle that reactivates the intrusive contact between the Mykonos laccolith and the overlying greenschist facies metabasites of the Upper Cycladic Unit. Structurally, above the Mykonos detachment is mainly a top-to-the-NE brittle structure marked by a 5–10-m thick cataclastic body and a conspicuous low-angle normal fault plane that puts late Miocene syn-rift sediments in direct contact with the Upper Cycladic Unit or directly with the Mykonos laccolith [*Avigad et al.*, 2001; *Sánchez-Gómez et al.*, 2002; *Lecomte et al.*, 2010]. A similar kinematics is observed at the scale of the island associated to ductile-to-brittle structures, indicating a continuum of deformation in the laccolith and the host rocks during their emplacement and the subsequent cooling. The NCDS likely accommodated  $\sim 30$  km of displacement after the intrusion of the Mykonos laccolith [*Brichau et al.*, 2008] with a progressive transfer from the Livada to the Mykonos detachment and a partly contemporaneous activity under brittle conditions [*Lecomte et al.*, 2010].

[10] The hydrothermal mineralization of Mykonos island belongs to the Aegean Cenozoic metallogenic province. It led to the development of a mining activity on the island with barite exploitation and processing by Mykobar Co. S.A. until 1984 and older small-scale sporadic mining for argentiferous galena, cerussite, anglesite, and iron hydroxides [Skarpelis, 2002]. The mineral deposits are mainly exposed in the central and the eastern parts of the island where they are preserved in the vicinity of the NCDS, indicating a probable close linkage with this major extensional structure (Figure 1). Skarpelis [2002] and Skarpelis and Gilg [2006] have distinguished two mineralization types on the basis of the occurrence mode, the ore mineralogy and textures and the origin of hydrothermal fluids. (1) A fragment-dominated sub-economic gold-enriched silica breccia along the Mykonos detachment cataclasite body (Figure 1b) that is filled with hydrothermal minerals including quartz with cockade, crustiform, and comb textures, as well as barite and minor relics of primary sulfides. Gold grades range up to 1 g/t [Skarpelis, 2002]. Fluid inclusions study on quartz shows evidence for boiling suggesting a depth of less than 1 km during mineralization [Skarpelis and Gilg, 2006]. Quartz was deposited from moderately saline, NaCl-dominated aqueous fluids (5–6 wt% total dissolved solids) at temperatures of ~230°C. (2) A sub-vertical NW–SE-trending barite

and Fe-hydroxide veins swarm that cuts the upper part of the Mykonos laccolith, the Upper Cycladic Unit, and the Miocene sediments that are besides heavily impregnated by the hydrothermal mineralization [Skarpelis, 2002; Lecomte et al., 2010]. The main banded texture of these veins indicates a successive deposition of the different mineralized contents during the vein opening. Fe-hydroxides and oxides as well as minor secondary Cu minerals result after oxidation of base-metal sulfides and carbonates that are preserved in the deeper parts of veins. Fluid inclusion data on vein barite indicate Ca-rich, highly saline fluids [Skarpelis and Gilg, 2006].

### 3. Detailed Mapping at the Vicinity of the NCDS on Mykonos

[11] In order to understand the interrelations between the mineralization on Mykonos island and the Aegean tectonics, we have carried out a new geological mapping (field mapping as well as satellite images analysis) of key areas (i.e., Cape Evros, Western coast of Panormos Bay, and Cape Haros) where both first-order structures (i.e., the detachments) and mineral deposits are spatially closely associated (Figure 1b).

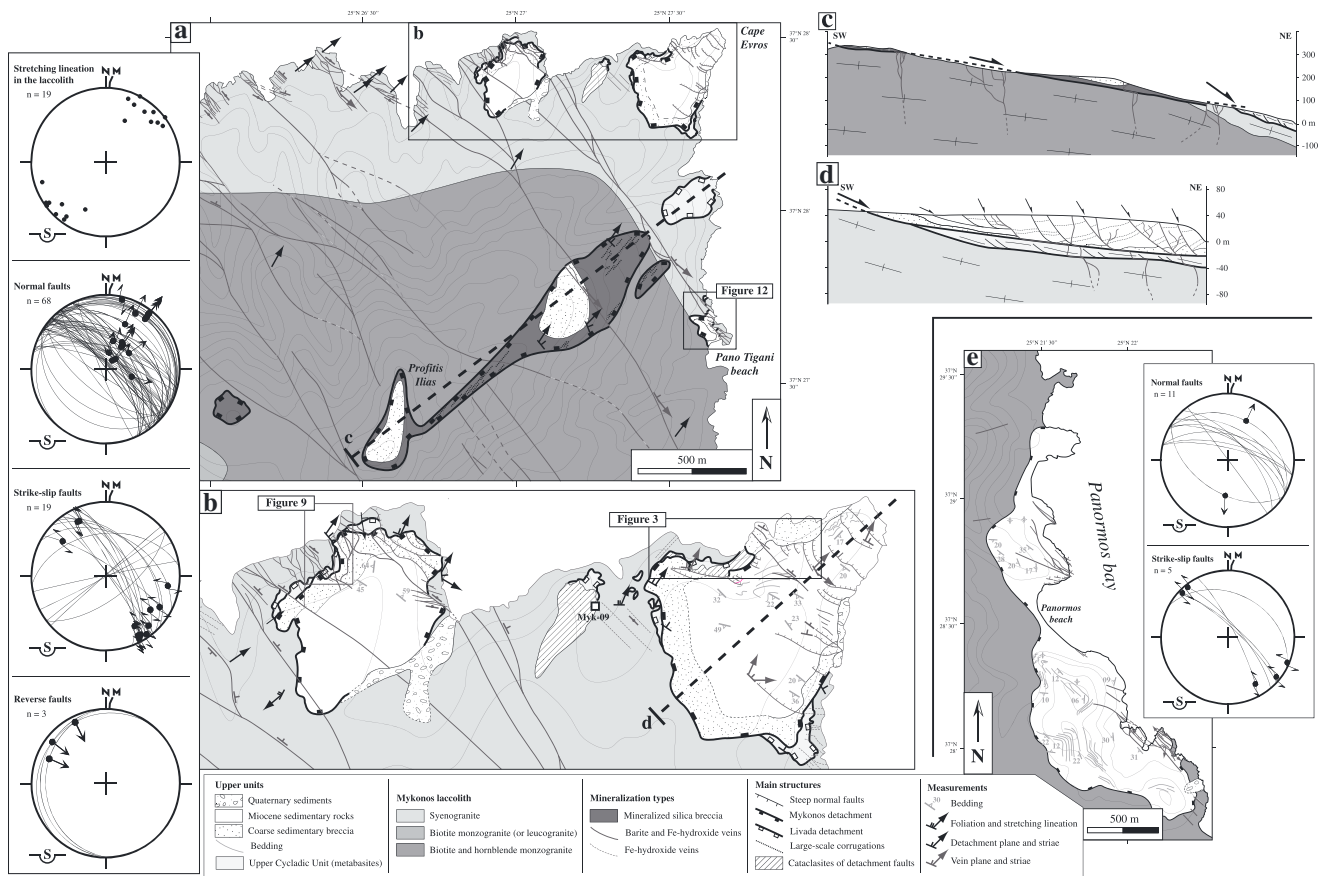


**Figure 2.** Field geological map of Cape Evros area and western coast of Panormos Bay. (a) Geological map of Cape Evros area. (b) Detailed geological map of Cape Evros area. (c and d) Cross-sections of Cape Evros oriented parallel to the stretching direction. (e) Geological map of western coast of Panormos Bay. See also Figure 1 for location. Fault and vein thicknesses are not to scale. The location of samples used for the chlorite geothermometry study is indicated (see results in Figure 10 and Table 1).

### 3.1. Cape Evros Area

[12] The first order geological mapping of the Livada and Mykonos detachments in Cape Evros area (Figure 2) was already well documented [Lecomte *et al.*, 2010]. The Livada detachment appears as a 10-m scale thick mylonitic shear zone developed at the contact between the Mykonos laccolith and the overlying Upper Cycladic Unit. There, the mylonitic foliation is shallow NE-dipping and carries a N30°E-trending stretching lineation with consistent top-to-the-NE kinematic indicators (Figure 2a) [Lecomte *et al.*, 2010]. Late steep and low-angle normal faults either cut or root within the detachment. Structurally, above the Mykonos detachment, roofing the Upper Cycladic Unit, displays a top-to-the-NE intensely hydrothermally altered cataclasite body (Figures 3a and 3b). Its hanging wall is made of syntectonic (i.e., syn-rift) sediments cut by numerous regularly spaced steep normal faults rooting into the detachment and defining a tilted-block geometry (Figure 3c). A 10–20-m thick coarse silicified sedimentary breccia marks the base of the sedimentary sequence. Due to intense normal faulting, the sediments can locally be in direct contact with the mylonitized laccolith with the tectonic omission of the Upper Cycladic Unit (Figure 3a).

[13] The hydrothermal mineralization in Cape Evros area occurs as barite and Fe-hydroxide impregnations in the late Miocene sedimentary unit and as mineralized silica breccia along the main fault zone of the Mykonos brittle detachment (Profitis Ilias; Figures 2 and 4). However, the main expression of this mineralization consists in banded barite and/or Fe-hydroxide veins forming a denser array close to the two branches of the NCDS (see details in part 3). These veins extend over 3 km along strike (Figure 2a). When the veins are emplaced along steep normal faults, they show a ~N110–140°E orientation with mainly a northeastward dip, while some of them may be associated with southwestward dipping antithetic faults (Figure 2). Other veins are also emplaced along strike-slip faults oriented N70–90°E and N120–140°E or within low-angle normal faults that may be reactivated with a reverse kinematics (see details in part 4).

### 3.2. Western Coast of Panormos Bay

[14] On the western coast of Panormos Bay (Figure 2e), the Mykonos detachment directly juxtaposes the syntectonic sedimentary unit over the top of the Mykonos laccolith through a several meters thick cataclasite zone. The bedding of the sediments dips toward the detachment plane forming a roll-over structure that indicates a flat-and-ramp geometry of the shallow-dipping detachment as described by Lecomte *et al.* [2010]. Numerous steep normal faults root into this first-order structure, affecting the late Miocene sediments.

[15] In this region, the veins present similar orientation (Figure 2e) and composition to those in Cape Evros area but are smaller and less abundant. Within the sediments, approaching the veins considered as feeders, the mineralization is often characterized by a pervasive impregnation or isolated geodic forms because of the replacement of the sedimentary matrix and former limestone pebbles of the conglomeratic layers by barite and/or goethite [Sánchez-Gómez *et al.*, 2002]. Moreover, the sediments display a clear color change from yellow- to red-colored, as a possible result of pyrite dispersion followed by supergene weathering to Fe-hydroxides, depicting large-scale halos in the vicinity of the veins.

### 3.3. Cape Haros Area

[16] Cape Haros area is mostly characterized by the Livada detachment that separates the Mykonos laccolith from the Upper Cycladic Unit (Figure 5). The best outcrop of the contact is exposed on the eastern side of Mersini Beach (Figure 6a). In the footwall, the highly deformed laccolith shows an alternation of shallow-dipping light-colored mylonites and dark ultramylonitic shear bands (Figure 6b). Within this mylonitic foliation, microscopic- to centimeter-scale kinematic indicators, such as shear bands and asymmetric pressure shadows on feldspar porphyroclasts, show a consistent NE–SW stretching lineation associated with an overall top-to-the-NE sense of shear (Figure 6c). In the hanging wall, the Upper Cycladic Unit also displays an intense ductile deformation with a strong foliation and meter-scale top-to-the-NE shear zones within a few meters above the contact. Foliation and shear planes are intruded by aplitic sills and dykes supporting the emplacement of the laccolith within the Upper Cycladic Unit during ductile deformation (Figure 6d). The hanging wall unit is also affected by numerous NW–SE-trending steep and low-angle normal faults that cut ductile structures and aplitic sills and root into or cut through the detachment, showing the superimposition of extensional brittle deformation onto ductile deformation. All these features are similar to the Livada detachment that crops out in the eastern part of Tinos island where the Upper Cycladic Unit and an intrusive granitoid dated at ~14 Ma are affected by a similar top-to-the-NE non-coaxial shearing [Faure *et al.*, 1991; Jolivet and Patriat, 1999; Brichau *et al.*, 2007; Jolivet *et al.*, 2010]. The late Miocene sedimentary unit is also observed as a small klippe surrounded by the Mykonos detachment on the west headland of Cape Haros (Figure 7a). The sedimentary unit, overlying the cataclastic Upper Cycladic Unit, is heavily affected by top-to-the-NE steep and low-angle normal faults mimicking at a smaller scale the detachment and associated tilted blocks observed at Cape Evros (Figure 7b).

[17] Similar to Cape Evros and Panormos Bay, the mineralization in Cape Haros area occurs mainly as ~N110–140°E sub-vertical veins (Figure 5) associated with, alternatively, normal and strike-slip kinematics. Some veins trend ~N70–90°E, in particular on Merchias peninsula where numerous small mineralized fault planes with a reverse kinematics are also observed (Figure 5d; see details in part 4).

## 4. Characterization of the Mineralization

### 4.1. Description of the Mineralization

[18] Both hydrothermal mineralization types described on Mykonos island [Skarpelis, 2002; Skarpelis and Gilg, 2006] are strongly structurally controlled. Indeed, the mineralization mostly occurs along sub-vertical NW–SE-trending veins with variable thickness from one centimeter to several meters (Figures 2, 4, 5, and 8a) containing banded barite and/or Fe-hydroxide, mainly goethite. Base-metal sulfides are preserved as patches at the deepest levels of the veins and comprise not only pyrite and marcasite with a colloidal texture (Figures 4 and 8b) but also arsenopyrite, chalcopyrite, galena, sphalerite, tennantite, tetrahedrite, boulangerite, geocronite, and jordanite [Skarpelis, 2002]. Quartz and carbonates, mainly siderite, occur as gangue, postdating the barite deposition with rare barite replacement by quartz (Figure 8c). The mineralization may

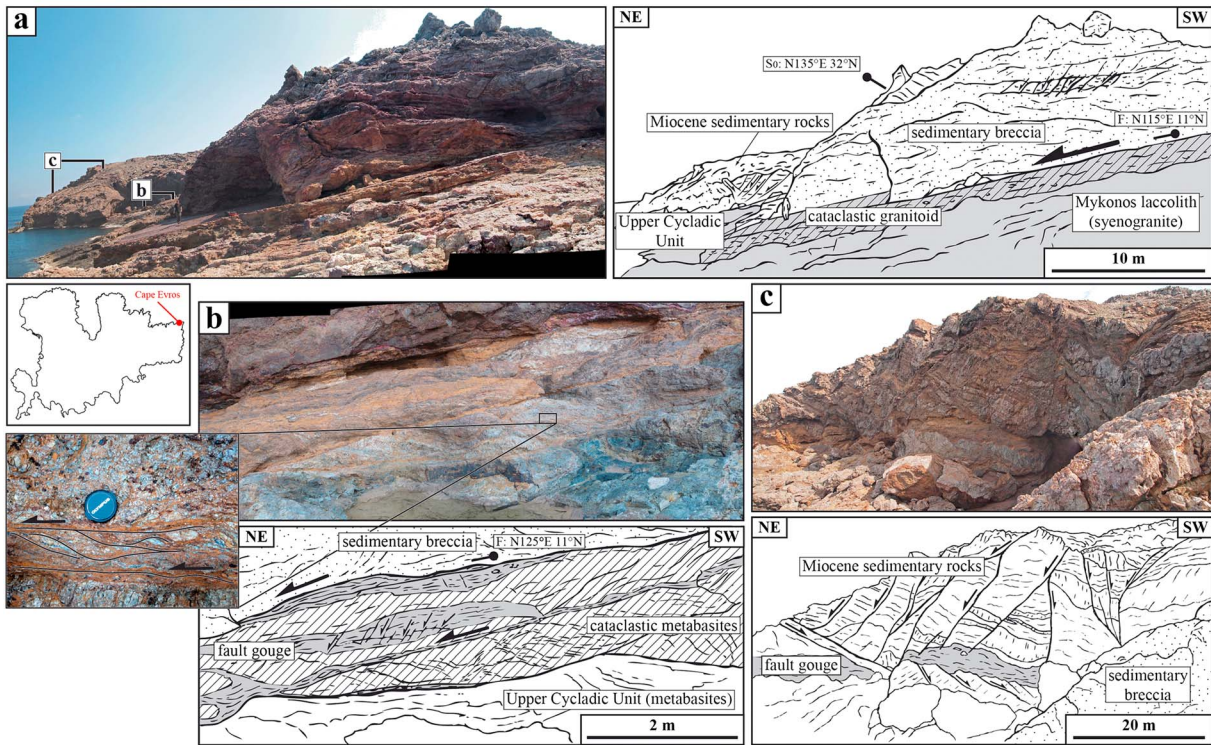


**Figure 3.** The Mykonos detachment in Cape Evros area. (a) Outcrop picture of the Mykonos detachment highlighted by a cataclasite body that puts the Miocene sediments in direct contact over the Mykonos laccolith. (b) Close-up view of the top-to-the-NE Mykonos detachment zone characterized by hydrothermal cataclasites and a fault gouge. (c) Tilted-block geometry in the Miocene sediments with normal faults rooting in the Mykonos detachment. See also Figure 2 for location.

also occur as a pervasive impregnation of Miocene sediments or as a silica coarse breccia within the Mykonos detachment cataclasite body (Figures 2a and 8d). In the latter, clasts in a Fe-hydroxide matrix are constituted by growth bands of quartz

and/or barite that can be replaced by quartz as in banded veins (Figure 8e). This breccia displays top-to-the-NE shear criteria compatible with the kinematics of the Mykonos detachment (Figure 8d).

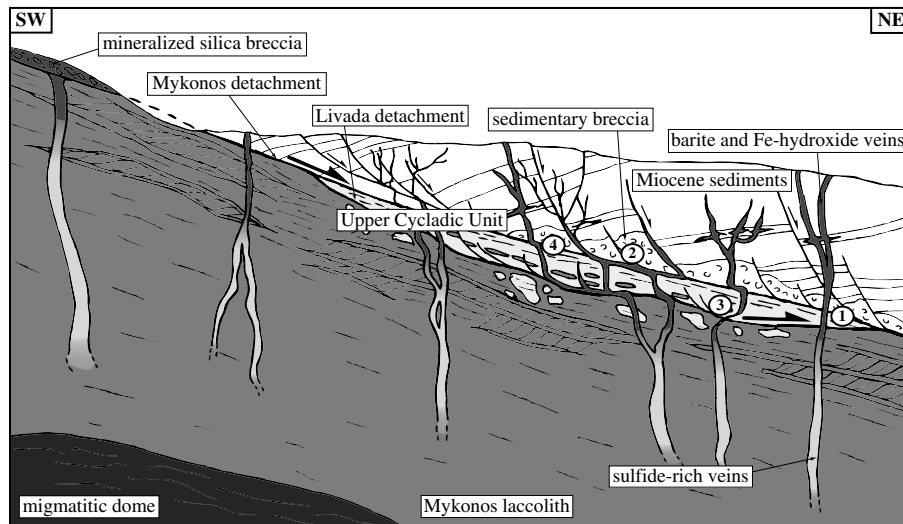


**Figure 4.** Interpretative diagram of Mykonos hydrothermal system in Cape Evros region showing the different morphologies of mineralization and the four different types of relationships between veins and detachments: (1) veins cut the detachment, (2) mineralization spreads out into the detachment, (3) veins sheared in the detachment, and (4) veins bent in the detachment. Gradual color change of veins corresponds to the evolution of the mineralized filling from sulfides to barite and Fe-hydroxides from the deeper to the upper parts of veins, respectively.

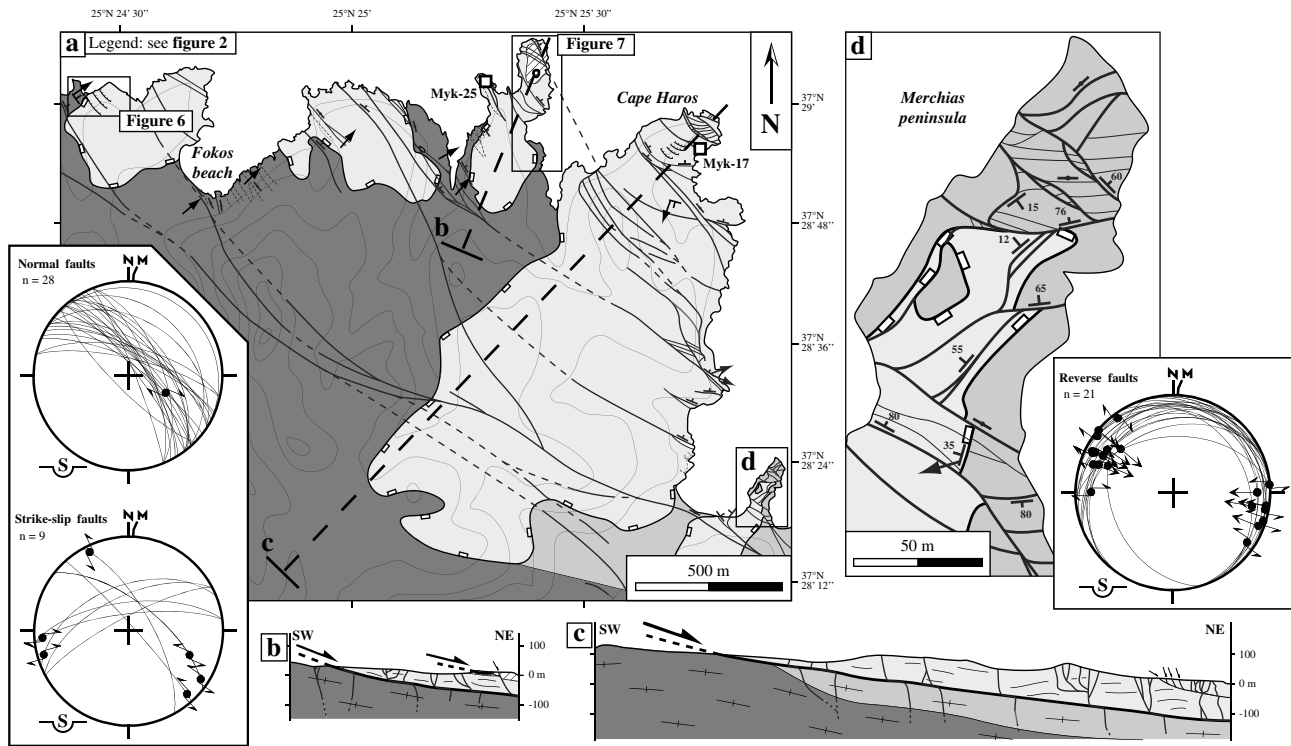


**Figure 5.** Field mapping of Cape Haros area. (a) Geological map of Cape Haros area. (b and c) Cross-sections of Cape Haros area parallel to the stretching direction. (d) Detailed geological map of Merchias peninsula. See also Figure 1 for location and Figure 2 for detailed legend. Fault and vein thickness is not at scale. The location of samples used for the chlorite geothermometry study is indicated (see results on Figure 10 and Table 1).

[19] The hydrothermal alteration in the Mykonos laccolith wall rocks is characterized by a pervasive silicification and an argillic and phyllic alteration resulting in the replacement of K-feldspar porphyroclasts mainly by kaolinite and sericite and the disappearance of biotite and amphibole (Figure 8f). The mylonitic fabric is however still preserved. In the Upper Cycladic Unit and in the cataclasites of the Mykonos detachment, this hydrothermal alteration is mainly marked by the crystallization of chlorite, quartz, and plagioclase in late fractures (Figure 8g).

[20] The mineralization develops exclusively in the vicinity of the NCDS (Figures 1b, 2, and 5) where veins display four different behaviors when they approach the Livada and Mykonos detachments. (1) Some steep veins cut across the detachments without any deflection or deformation (Figure 9a). (2) Other veins spread out into the detachment zone from steeply-dipping feeders (Figure 9a). Then, the mineralization is often brecciated (Figure 8d) and the mineralized planes are striated. (3) Some veins are sheared and their mineralogical content is deformed in agreement with the kinematics of the detachments (Figure 9b). (4) Finally, many veins show an apparent top-to-the-SW bent shape when they cut across the detachment or within the sedimentary breccia, which appears inconsistent with the top-to-the-NE fault kinematics (Figures 9c and 9d). In this case, barite crystals are devoid of deformation.

**4.2. Temperature Conditions of Mineralization Emplacement**

[21] Hydrothermal chlorite associated with the mineralization (Figure 8g) provides a useful tool to estimate the temperature that prevailed when the hydrothermal fluid

interacted with the host rocks. Accordingly, different chlorite geothermometers have been used. (1) The two thermometers of *Cathelineau and Nieva* [1985] and *Cathelineau* [1988] based on the study of the active geothermal system of *Los Azufres* (Mexico), which use the variation in Al(IV) and octahedral vacancies (VI(vac)) in chlorite crystal lattice, are correlated with the crystallization temperature. In these examples, host rocks are constituted by zeolite-, greenschist-, and amphibolite-facies andesites, containing hydrothermal chlorite crystals, associated notably with quartz and epidote. (2) The thermometer of *Kranidiotis and MacLean* [1987] that correlate the temperature of hydrothermal chlorite crystallization in rhyodacite to rhyolite host rocks with the Al(IV) content and the Fe/(Fe + Mg) ratio, particularly within the assemblage quartz-chlorite ± sericite.

[22] These geothermometers are valid for specific mineral phase equilibrium and host rock type because they are based only on substitutions in the chlorite crystal lattice that can depend upon other factors than temperature. The pH of the coexisting fluid [*Walshe*, 1986], the presence of other minerals between chlorite layers [*Jiang et al.*, 1994], and the nature and therefore the chemistry of the wall rock also have an influence on chlorite composition. Thus, the use of chlorite geothermometry using data from phase equilibrium experiments [*Vidal et al.*, 2001] seems more appropriate.

[23] In this work, chemical analyses of chlorites crystals have been performed on a Cameca SX50 electron microprobe at the University Pierre et Marie Curie (Paris VI). Analytic conditions were 15 kV accelerating voltage and 12 nA beam current using Fe<sub>2</sub>O<sub>3</sub> (Fe), MnTiO<sub>3</sub>

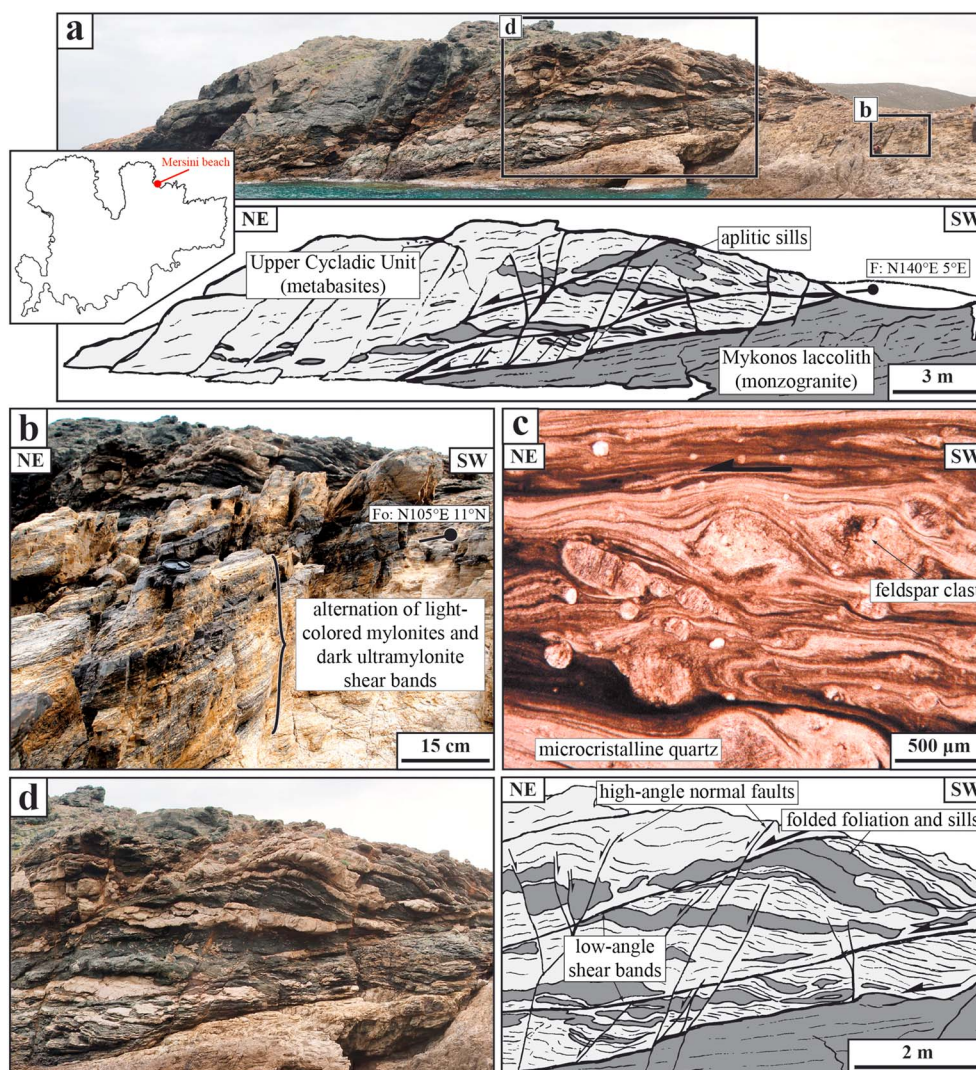


**Figure 6.** The Livada detachment in Cape Haros area. (a) Landscape picture of the Livada detachment cropping out close to Mersini beach. (b) Close-up view of shallow dipping ductile deformation of Mykonos laccolith close to the Livada detachment. (c) Microscopic view of top-to-the-NE shearing criteria within the mylonitic zone of the laccolith (polarized transmitted light). (d) Detail of intruded aplitic sills in the Upper Cycladic Unit and top-to-the-NE ductile-brittle extensional deformation associated to the Livada detachment. See also Figure 5 for location.

(Mn, Ti), diopside (Mg, Si),  $CaF_2$  (F), orthoclase (Al, K), anorthite (Ca), albite (Na), and vanadinite (Cl) as standards. The counting time was 10 s for all elements. Two types of hydrothermal chlorite crystals have been analyzed: The first type is chlorite crystallizing with quartz and plagioclase in fractures that developed close to barite veins (Figure 8g) within the Upper Cycladic Unit (i.e., metabasites; Myk-25 and Myk-17 samples; Figure 5a). Their composition, enriched in  $Al_2O_3$ , evolves between amesite and sudoite end-members (Figure 10) and their  $Fe/(Fe + Mg)$  ratio evolves from 0.37 to 0.45. (2) The second type is chlorites formed within the cataclasites of Mykonos detachment associated with quartz (Myk-09 sample; Figure 2b). Richer in  $SiO_2$ , these chlorite crystals are comprised between the clinocllore-daphnite and the sudoite end-members (Figure 10) and their  $Fe/(Fe + Mg)$  ratio is higher, comprised between 0.43 and 0.5.

[24] Both types of hydrothermal chlorite crystals display Si (IV) content from 5.6 to 6.6 cations per formula unit, that is too high to use Fe-Mg aluminous chlorite geothermometer of Vidal *et al.* [2001]. Crystallization temperatures for the hydrothermal chlorites obtained with the other geothermometers yield a consistent 250–282°C narrow range of temperature in the Upper Cycladic Unit and a lower temperature range of 203–258°C in the cataclasites (Table 1).

[25] This variability is not necessarily the result of different hydrothermal fluid temperatures but can be related to the variable chemistry of the Upper Cycladic Unit and the cataclasites. Nevertheless, the temperature range obtained with chlorite geothermometers is in agreement with the study of fluid inclusions in quartz of the mineralized breccia that yielded a temperature of ~230°C [Skarpelis and Gilg, 2006].

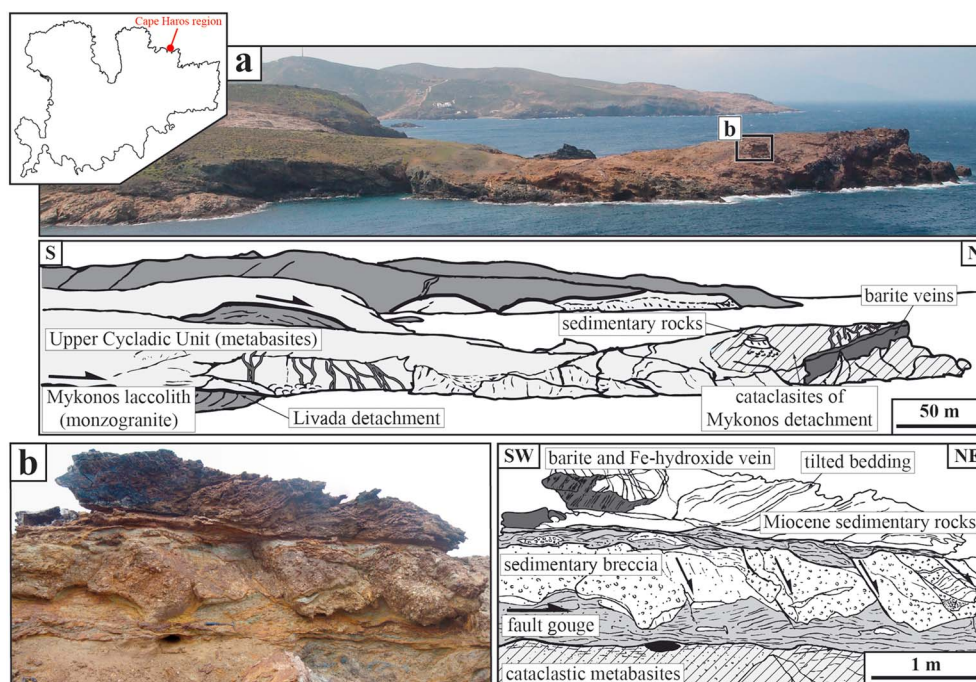


**Figure 7.** The Mykonos detachment in Cape Haros area. (a) Northern coast of Cape Haros area showing the Livada and Mykonos detachments. (b) Tilted-block geometry within the Miocene sediments in the hanging wall of the Mykonos detachment. See also Figure 5 for location.

## 5. Evidence of Successive Tectonic Regimes

### 5.1. Magmatic to Ductile Deformations

[26] The sub-solidus deformation of the Mykonos laccolith is mainly observed in the root zone of the intrusion toward the SW of the study area (Figure 1b). It is characterized notably by a plano-linear magmatic fabric of K-feldspars that is strictly parallel to the ductile fabric of the host migmatitic dome, suggesting a syn-extensional emplacement of the laccolith [Faure and Bonneau, 1988; Faure et al., 1991; Denèle et al., 2011]. The magmatic deformation in the laccolith evolves to a post-solidus deformation forming protomylonitic structures close to the migmatitic dome to ultramylonitic ones in the vicinity of the Livada and Mykonos detachments. Mineral foliation is oriented NW–SE and displays a shallow dip to the NE. The mineral or stretching lineation trends from  $\sim$ N90°E in the west of the laccolith toward  $\sim$ N30–20°E close to the NCDS (Figure 1b). Furthermore, numerous kinematic indicators, such as asymmetric folding of the mylonitic foliation, shear bands and asymmetric pressure shadows around porphyroclasts within the mylonitic laccolith and the Upper Cycladic Unit, are consistent with a top-to-the-NE sense of the ductile shear (Figure 6c).

### 5.2. Brittle Deformation and Relationships With the Mineralization

[27] The brittle deformation is well developed, particularly in contact zones between distinct tectonic units where it partly overprints the ductile structures. The Livada detachment is thus locally reworked by a set of low-angle and steep normal faults rooting into or cutting the contact with the Mykonos laccolith (Figure 6). The Mykonos detachment is exclusively a brittle structure with a thick cataclasite zone

and numerous steep normal faults defining a tilted-block geometry (Figures 3 and 7). At the scale of Mykonos island, the strike of these faults that are often mineralized is broadly comprised between N110°E and N150°E with a variable northeastward dip (i.e., 10° to sub-vertical) accompanied by a subordinate set of southwestward dipping faults (Figures 2 and 5). No significant fault orientation variations have been observed between the different regions of the island, and the strike of these extensional faults is consistent with the NE–SW direction of regional stretching (Figures 2 and 5) [Gautier and Brun, 1994a; 1994b; Avigad et al., 1998]. However, a second set of faults is observed in zones where the veins network is particularly developed. For instance, on Merchias peninsula, N70–90°E-trending veins are conjugated with  $\sim$ N130°E-trending ones while they both carry sub-horizontal striations (Figure 5d).

[28] Striations on the fault planes are complex with several generations of striae related to a succession of different stress regimes. NW–SE-trending mineralized steep fault planes associated with different mineralization stages display (1) NE–SW dip-slip striae and normal kinematic indicators and (2) sub-horizontal NW–SE striae that show a strike-slip movement (Figure 11a). On low-angle fault planes and notably on the Mykonos detachment plane, two generations of striae are observed: (1) a 10-m scale corrugation accompanied at small scale by a well-marked striation broadly oriented NE–SW and compatible with the top-to-the-NE main extensional movement of the detachment (Figure 2a) and (2) E–W to NW–SE striae associated with reverse kinematic indicators (Figures 5d and 11b).

[29] The overall geometry of veins is also variable and can be used as a strain marker. Indeed, in contrast with most of NW–SE banded veins formed as pure tension gashes

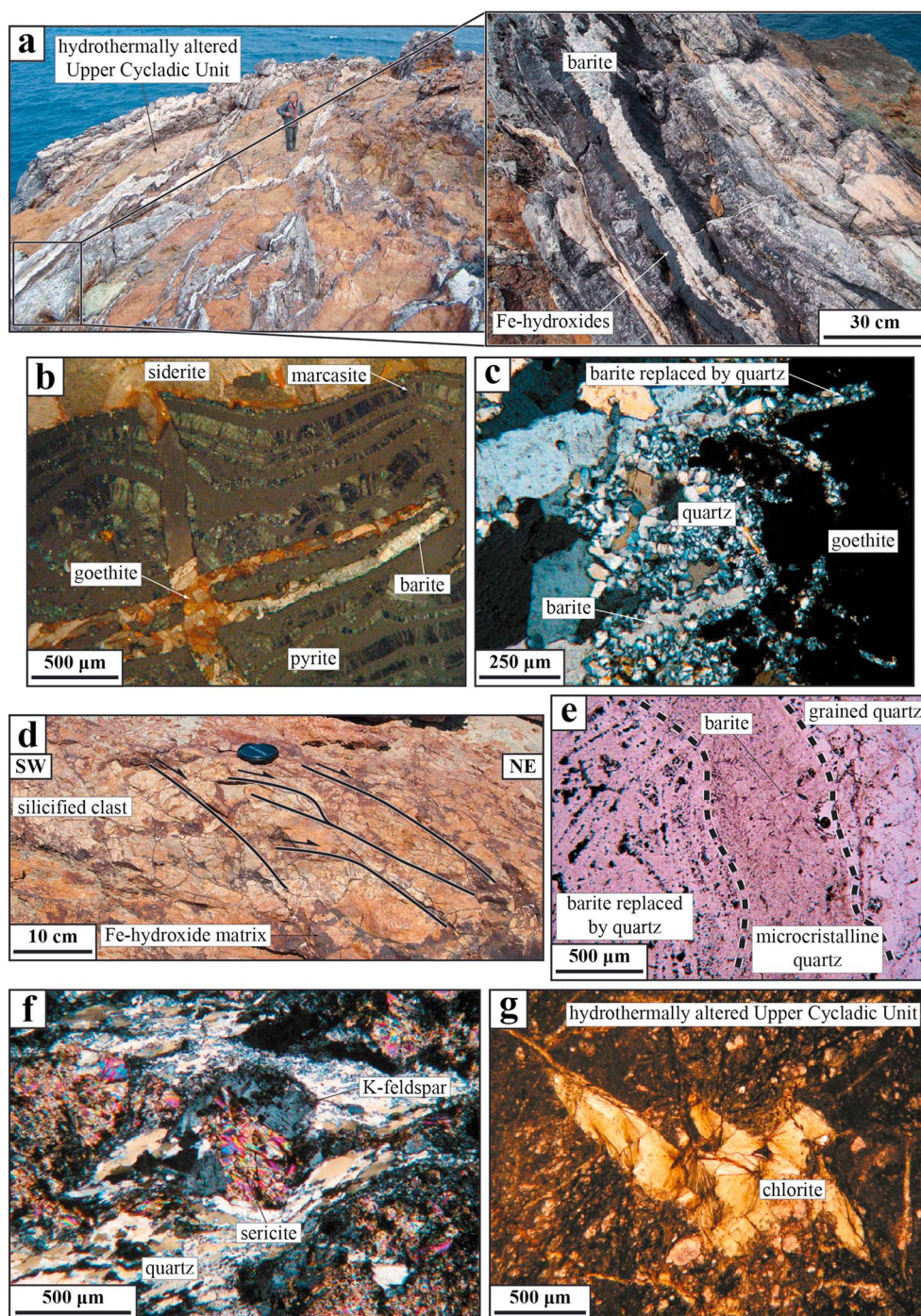


**Figure 8.** Different morphologies of hydrothermal mineralization and associated hydrothermal alterations. (a) Sub-vertical banded barite and Fe-hydroxide veins network (Cape Haros area). (b) Microscopic view of sulfide mineralization in veins with colloidal pyrite and marcasite crosscut by siderite, barite, and goethite (polarized analyzed reflected light). (c) Microscopic view of banded filling of veins with barite, goethite, and quartz that may replace barite crystals (polarized analyzed transmitted light). (d) Top-to-the-NE shearing criteria in mineralized silica breccia (Cape Evros area). (e) Microscopic view of growth bands of quartz and/or barite of clasts in mineralized breccia (polarized transmitted light). (f) Microscopic view of phyllic alteration of K-feldspars of mylonitic laccolith (polarized analyzed transmitted light). (g) Microscopic view of hydrothermal chlorites in metabasites of Upper Cycladic Unit (polarized transmitted light).

(Figure 8a), other veins, filled with barite or collapse breccia with Fe-hydroxide matrix, display a clear pull-apart morphology compatible with a left-lateral slip for  $\sim N130^\circ E$  veins (Figure 11c) or a right-lateral one for  $\sim N80^\circ E$  structures (Figure 11d) forming an obvious conjugate strike-slip faults system (Figure 11e).

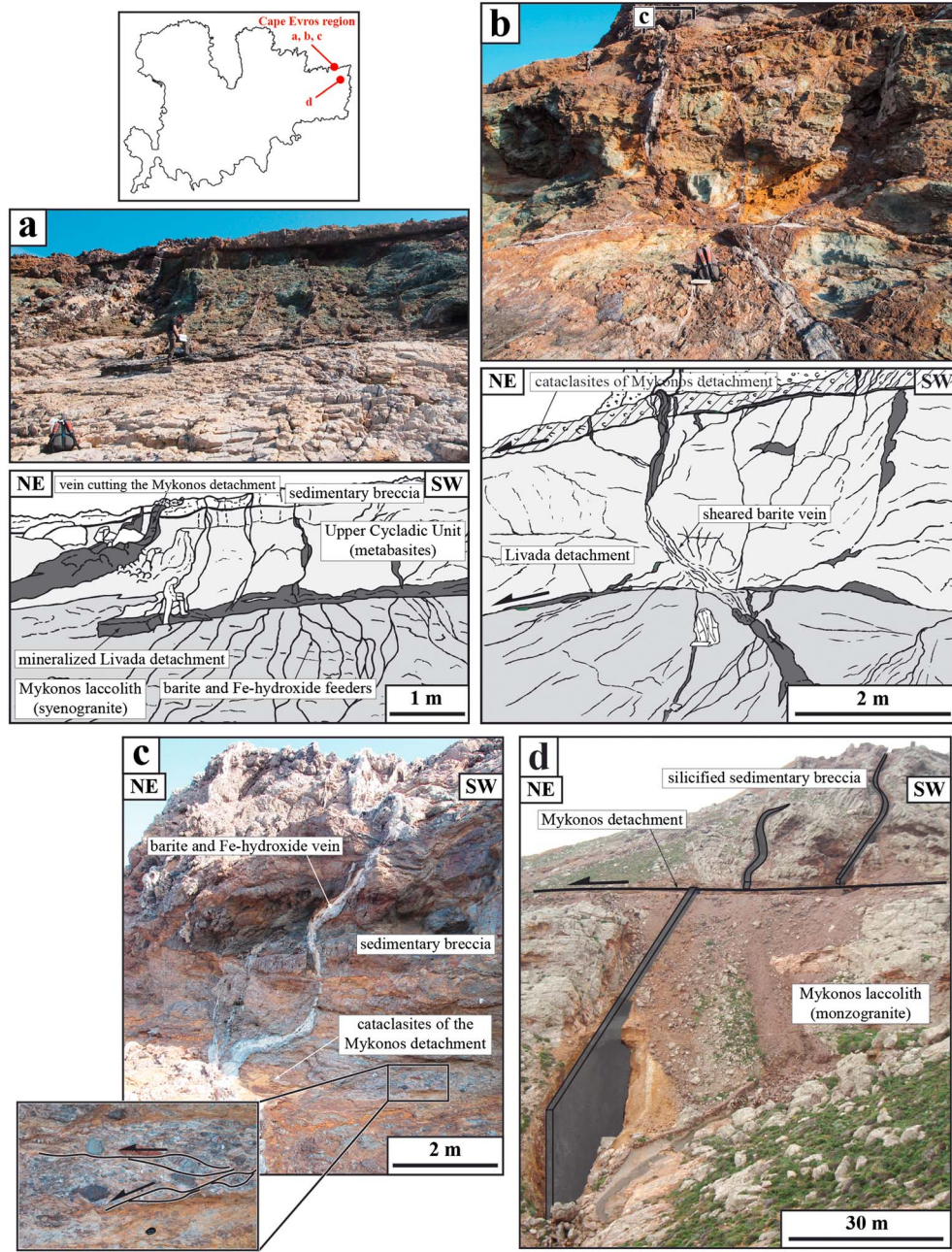


**Figure 9.** Relationships between veins and detachments. (a) Barite and Fe-hydroxide veins spreading out in the Livada detachment or crosscutting the Mykonos detachment. (b) Top-to-the-NE sheared vein in the Livada detachment. (c) Vein bent in the Mykonos detachment. (d) Exploited vein bent at mining-work scale. See also Figure 4.

### 5.3. Chronology of the Deformation

[30] As described above, the ductile deformation, observed in the laccolith and surrounding units, is characterized by an NE-shallow dipping foliation and an NE–SW mineral and stretching lineation associated with a top-to-the-NE kinematics (Figure 1b). The Livada detachment between the laccolith and the Upper Cycladic Unit also displayed a ductile activity with the development of top-to-the-NE ductile shear bands (Figure 6). As no significant post-slip tilt of these structures is observed [Lecomte *et al.*, 2010], this deformation is considered as purely extensional.

[31] Then, extensional brittle deformation developed with the reactivation of the Livada detachment and the inception of the Mykonos detachment as top-to-the-NE low-angle normal faults (Figures 3, 6, and 7). Syn-sedimentary NW–SE high-angle normal faults also formed, affecting the Upper Cycladic Unit and the Mykonos laccolith as well as the Miocene sediments. The first-order structure defines a tilted-block geometry compatible with the top-NE motion along the NCDS (Figures 3, 7, and 13a).

[32] Afterward, the low-angle normal faults were cut by strike-slip faults. This feature is particularly well exposed along the eastern coast of Cape Evros area, close to Pano Tigani

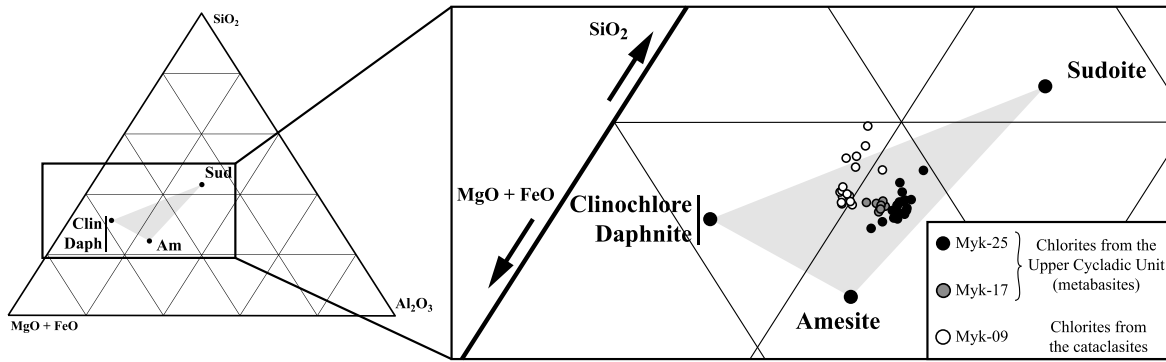


**Figure 10.** SiO<sub>2</sub>-Al<sub>2</sub>O<sub>3</sub>-FeO+MgO diagram showing the chemical variations of the studied hydrothermal chlorites.

beach (Figure 12a). Indeed, on this outcrop, the Mykonos detachment is dissected by a set of conjugate strike-slip faults (Figures 12b and 12c) and displays a staircase morphology, resulting from a minor vertical component of the dominant left-lateral motion (Figure 12d). Fault planes are often mineralized with several strike-slip striae generations, associated with different pulses of hydrothermal mineral deposition (Figure 12c). These strike-slip faults both reactivated the NW–SE normal faults with a component of left-lateral slip (Figures 11c and 12c) or formed as new fault segments with NE–SW right-lateral slip component (Figure 11d). Moreover, field observations at Cape Evros show that individual faults display evidence for polyphase overprinting by strike-slip and dip-slip extensional kinematic indicators (Figure 11a). This succession indicates that extensional regime alternated with the strike-slip regime during this stage.

[33] The development of small-scale reverse faults (Figure 11b) is in agreement with a late reactivation of the detachments, highlighted on Pano Tigani outcrop. Indeed, the Mykonos detachment plane shows post-mineralization E–W- to NW–SE-trending reverse striae superimposed on the NE–SW extensional kinematic indicators (Figure 12e). In this case, strike-slip faults are also cut by the reworked detachment (Figure 12e).

## 6. Interpretations and Discussion

### 6.1. Interrelations and Timing of Mykonos Laccolith Emplacement, Extensional Structures, and Mineralization Deposition

[34] In this study, numerous features show a close linkage of the mineralization and extensional structures: (1) the massive concentration of mineralization in the vicinity of the Livada and Mykonos detachments (Figure 1) demonstrating the ability of these zones to channelize fluid flow as described by *Reynolds and Lister* [1987] in the Basin and Range province, (2) the NW–SE preferential orientation of veins (Figures 2 and 5) and their internal banded texture (Figure 8a) showing that the vein opening is primarily controlled by the NE–SW stretching of the crust, and (3) the different vein geometries (Figures 4 and 9) when these structures interact with the two branches of the NCDS, showing that the mineralization stage lasted during and partly after the extensional brittle activity of the Livada and Mykonos detachments. Indeed, the mineralized veins

that are sheared with top-to-the-NE sense along the detachment are tectonically brecciated with angular fragments (Figures 8d and 9b) while other veins cut across these first-order structures (Figure 8a). Moreover, the apparent top-to-the-SW bent shape of many undeformed veins (Figures 9c and 9d) can support the syntectonic deposition of the mineralization. Indeed, one hypothesis to explain this phenomenon is to consider a rotation of principal stresses  $\sigma_1$  and  $\sigma_3$  within the detachment zone during its activity as suggested by *Lecomte et al.* [2011]. Thus,  $\sigma_1$ , vertical outside the fault zone, adopts a shallower attitude compatible with both the sense of slip along the fault and the opening of the veins [*Lecomte et al.* 2011, Figure 6]. Another hypothesis is to consider the detachment as a shear zone with a strong coaxial component. However, in this case, the mineralogical content of the vein would be deformed while those bent veins are undeformed (Figure 9c). Thus, according to the first hypothesis, a part of the mineralization occurred contemporaneous with the activity of the NCDS and therefore at the end of the emplacement and cooling of the Mykonos laccolith considering that veins cut the intrusion. The thickness of mineralized zone (i.e., the depth of influence of the veins below the detachments) can be estimated considering the westernmost limit of outcropping veins in Cape Evros and Cape Haros area (Figure 1b) and the shallow dip of the mylonitic foliation. Indeed, this foliation and the veins are all related to the detachments activity. Thus, considering the amount of eroded material, the dip of the foliation and detachments and the hor-

**Table 1.** Mean Chlorite Crystallization Temperatures Obtained With Different Chlorite Geothermometers<sup>a</sup>

Locality	T <sub>1</sub> (°C)	T <sub>2</sub> (°C)	T <sub>3</sub> (°C)
Myk-25 (Figure 5a) Hydrothermally altered metabasites 20 analyses	251 (17)	260 (10)	282 (17)
Myk-17 (Figure 5a) Hydrothermally altered metabasites 8 analyses	250 (5)	271 (3)	278 (5)
Myk-09 (Figure 2b) Hydrothermally altered cataclasites 16 analyses	203 (32)	258 (17)	236 (32)

<sup>a</sup>T<sub>1</sub>: Al(IV) thermometer. T<sub>2</sub>: VI(vac) thermometer [*Cathelineau and Nieva*, 1985]. T<sub>3</sub>: Al(IV) and Fe/(Fe+Mg) thermometer [*Kranidiotis and MacLean*, 1987]. Standard deviation is indicated in italic.

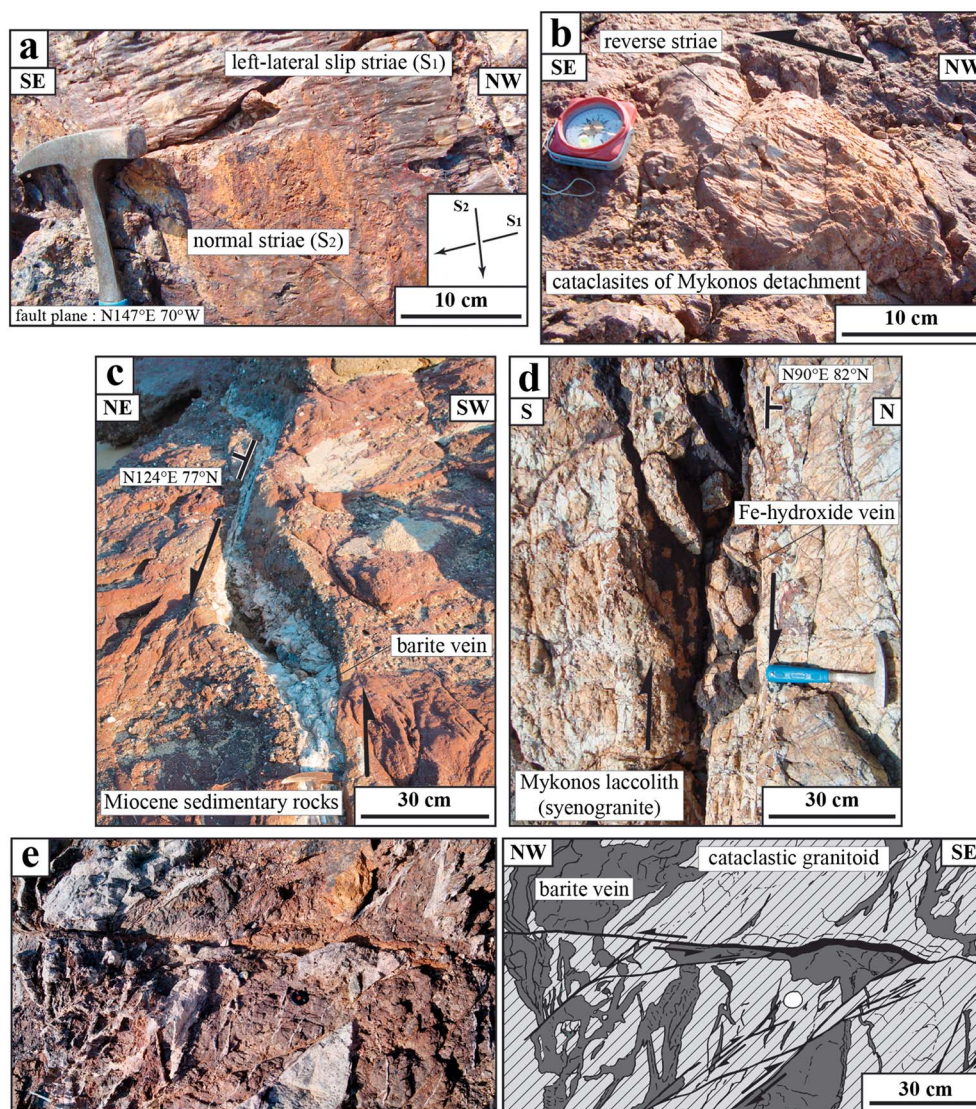


**Figure 11.** Deformation that affects the veins. (a) Mineralized fault plane showing a first left-lateral slip striae generation associated to quartz and a second normal one associated to Fe-hydroxides (Cape Evros area). (b) Indications for reverse kinematics on minor shallow-dipping fault planes (Cape Evros area). (c and d) Indications for strike-slip kinematics with left-lateral and right-lateral slip pull-aparts (Cape Evros and Panormos area). (e) Conjugate strike-slip faults system (Cape Evros area).

horizontal distance to the westernmost vein, maximal depth can be crudely estimated to 700 m, measured perpendicular to the NCDS (Figure 1c).

[35] The emplacement at shallow depth of the hydrothermal mineralization suggested by *Skarpelis and Gilg* [2006] involves meteoric or connate fluids at near-hydrostatic pressure channeled by deviatoric stress-dependant open tensile fractures [Reynolds and Lister, 1987]. These conditions occur in the shallower segments of the detachment system above the ductile-brittle transition and are confirmed in our study by the preferential orientation of veins (Figures 2 and 5). Indeed, high fluid pressure that occurs below the ductile-brittle transition, where less-oxidized igneous-derived fluids dominate [Reynolds and Lister, 1987], would have preferentially induced a dispersion of vein orientations. Thus, when the laccolith crossed the ductile-brittle

transition, an intense fracturing occurred favoring fluid-rock interactions within the pluton and the development of convection cells between the magmatic intrusion and the overlying basin. These modifications of the physico-chemical conditions of the hydrothermal fluids may finally result in a decreasing of metals solubility. Thus, the mineralizing episode probably occurred after this major change until shallow crustal levels. On the basis of variation of fluid inclusions composition, *Skarpelis and Gilg* [2006] have interpreted the veins and the brecciated mineral deposit as two different mineralizing stages. However, these fluid inclusions come from different mineral phases, and this variation is possibly a result of a late hydrothermal fluid modification due to a possible leakage of fluid in barite inclusions [Skarpelis and Gilg, 2006]. Thus, a single mineral deposition stage may also be envisaged notably due to the

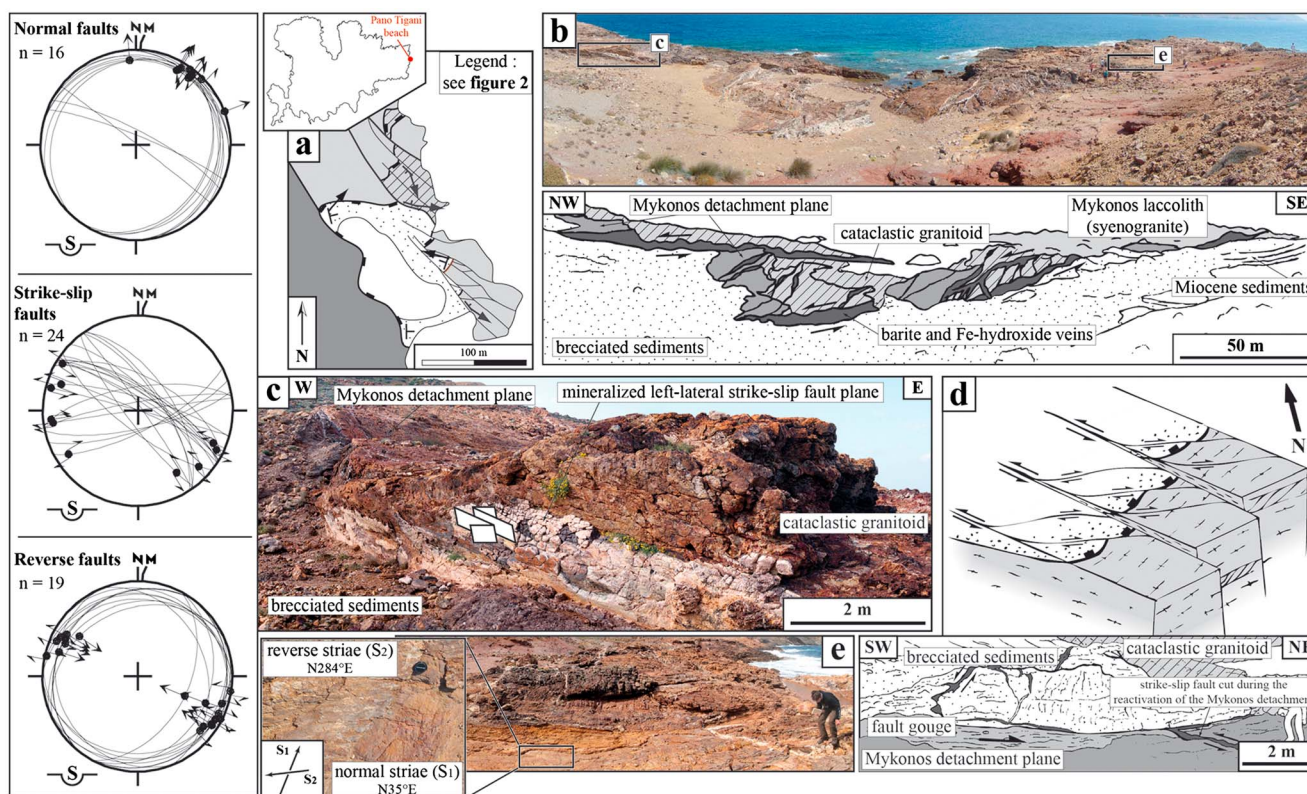


**Figure 12.** Deformation of the Mykonos detachment in Pano Tigani area. (a) Geological map of Pano Tigani area. (b) Panorama of Pano Tigani outcrop with the Mykonos detachment dissected by strike-slip faults. (c) Mineralized left-lateral slip fault plane dissecting the Mykonos detachment. (d) 3-D diagram synthesizing the brittle deformation observed on Pano Tigani area. (e) Barite vein with reverse striae spreads out in the Mykonos detachment plane. See Figure 2 for location and detailed legend.

similar mineral phases observed in the veins and in the mineralized breccia (i.e., succession of barite and quartz stages with possibly a replacement of barite by quartz; Figures 8c and 8e).

## 6.2. Age of the Mineralization Emplacement

[36] One of the available models for the formation of hydrothermal ore deposits in detachment zone involves convective fluid flow related to the cooling of a magmatic intrusion. Indeed, the pluton provides heat causing a local steepening of the geothermal gradient and that animates convection cells [Reynolds and Lister, 1987]. Using cooling curves of the laccolith in the footwall of the Mykonos detachment defined from a wide range of thermochronometric data [Brichau *et al.*, 2008], the age of barite veins deposition may be estimated assuming that the mineralizing fluids are in thermal equilibrium with the laccolith. Plotting the range of temperatures obtained above for the hydrothermal chlorite crystallization (i.e., 280 and 200°C; Table 1) on the time-temperature diagram (Figure 14), the emplacement age of the mineralization occurred in narrow range between 11 and 10 Ma. This temperature range is consistent with the closure temperature for zircon fission tracks at moderate-to-fast cooling rate (i.e.,  $280 \pm 30^\circ\text{C}$ ), which besides fits well with the lower temperature bound of the ductile-brittle transition (Figure 14) [Stöckhert *et al.*, 1999]. Therefore, a similar ~11–10 Ma age may be proposed for the crossing of ductile-brittle transition by the Mykonos laccolith. This age must be considered as

the oldest possible age of the mineralization emplacement if the wall rock is not hotter than the mineralizing fluids.

[37] This age is also consistent with (1) a part of the timing of the NCDS activity (14 to 10 Ma for the Livada detachment and 14 to 9 Ma for the Mykonos detachment) [Brichau *et al.*, 2008; Jolivet *et al.*, 2010] and therefore with the syntectonic nature of the mineral deposition and (2) with the timing of the sediments deposition. Indeed, the mineralization is not observed in the upper part of the sedimentary unit while sedimentation continued in the basin until a maximum age of 9–8 Ma, as attested by the 10 Ma old granitoid clasts observed on the top of the conglomeratic sequence [Sanchez-Gómez *et al.*, 2002].

## 6.3. Temporal Evolution of the Stress Regime

[38] On Mykonos island, previous studies have highlighted an evolution of the deformation, particularly within the Mykonos laccolith, with the development of first magmatic, then ductile and finally brittle extensional fabrics [Faure and Bonneau, 1988; Lee and Lister, 1992; Lucas, 1999; Lecomte *et al.*, 2010; Denèle *et al.*, 2011]. This study shows that final cooling of the Mykonos laccolith was characterized by a progressive change in stress regime contemporaneously with the mineral deposition 11–10 Ma ago (Figures 13a and 14).

[39] Based on these new structural observations, faults and/or veins systems have been systematically measured (Figures 2, 5, and 12). With the strike, dip, and striae data

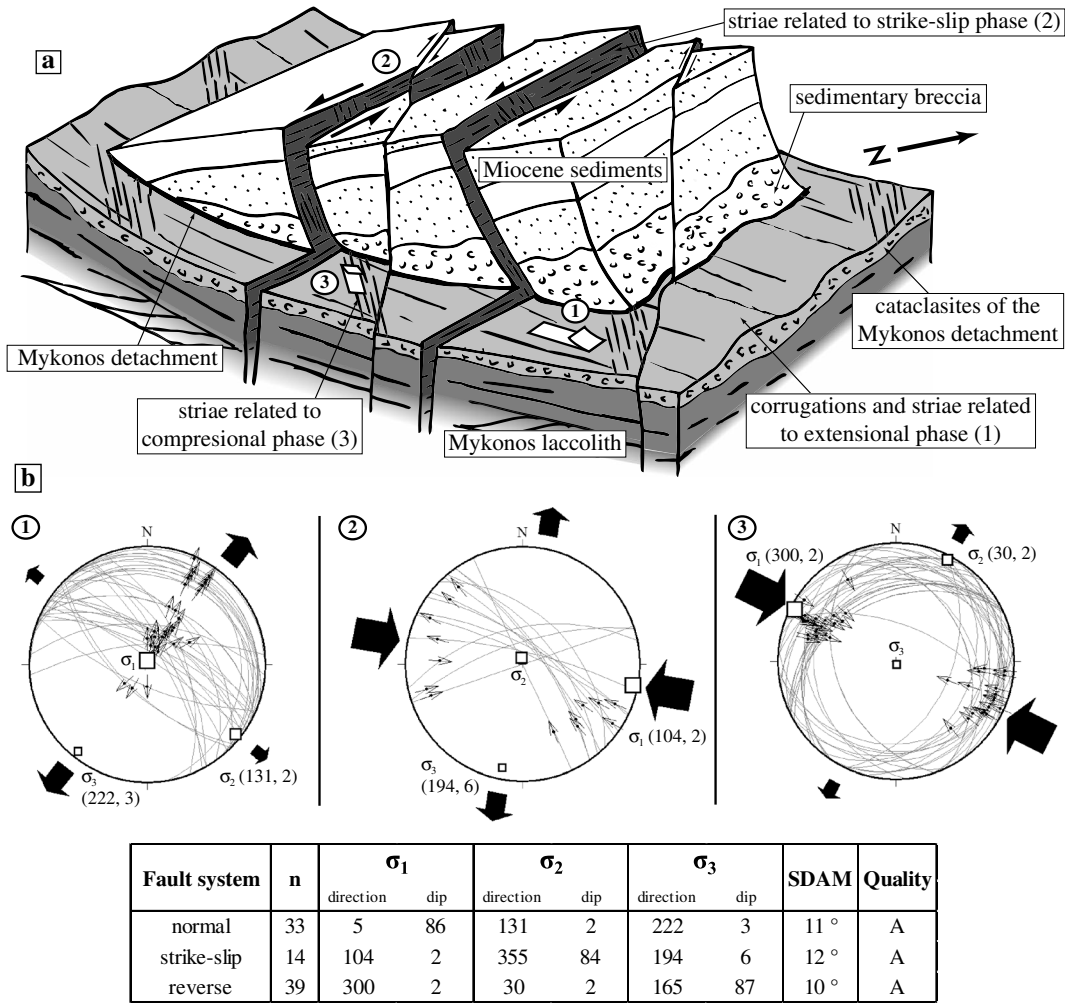


**Figure 13.** Evolution of the stress regime on Mykonos island. (a) 3-D diagram showing the ductile and brittle deformation related to the three successive stress regimes. (b1–b3) Palaeostresses results for normal, strike-slip, and reverse faults systems, respectively. Table shows detailed results of palaeostress study. n: number of structural data. SDAM: Standard Deviation of Angular Misfit. Quality A: well-defined palaeostresses.

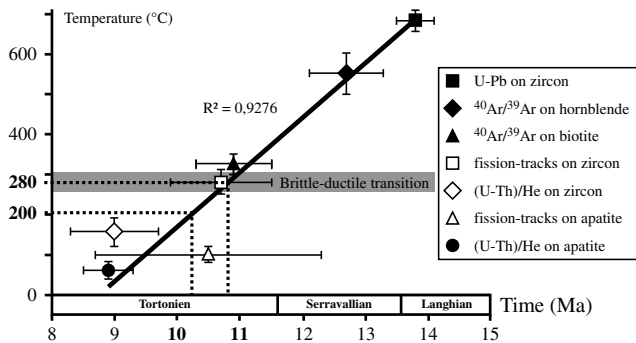


**Figure 14.** Time-temperature diagram showing the cooling curve of Mykonos laccolith in the footwall of the Mykonos detachment (modified from Brichau et al. [2008]). The error bars on both ages and temperatures are at  $2\sigma$ . The inferred timing for chlorite crystallization is indicated. The temperature of the ductile-brittle transition is according to Stöckhert et al. [1999].

collected, we have isolated different sets of faults in order to define the palaeostress orientation patterns by computer-aided inversion method (*T-Tecto 3.0* software [Zalohar and Vrabec, 2007]) described in details by Angelier [1979, 1994]. Three successive stress tensors have been distinguished. For each of them, the observation that the principal stresses are close to theoretical directions (i.e., two horizontal principal stresses and one vertical one) and the standard deviation of angular misfit parameter (SDAM, equivalent to the ratio  $\nu$  parameter of the direct inversion method [Angelier, 1994]) ensures the reliability of the result (Figure 13b).

[40] First, for the normal faults system with both detachment planes and steep normal faults that are oriented  $\sim\text{N}110\text{--}140^\circ\text{E}$ , the palaeostress analysis indicates a vertical  $\sigma_1$  with  $\sigma_2$  and  $\sigma_3$  oriented  $\text{N}128^\circ\text{E}$  and  $\text{N}219^\circ\text{E}$ , respectively. Then, for the strike-slip faults system with two different orientations ( $\sim\text{N}80^\circ\text{E}$  and  $\sim\text{N}100\text{--}140^\circ\text{E}$ ) that correspond to right- and left-lateral strike-slip faults, respectively, the inversion reveals a stress regime characterized by a vertical  $\sigma_2$  with  $\sigma_1$  and  $\sigma_3$

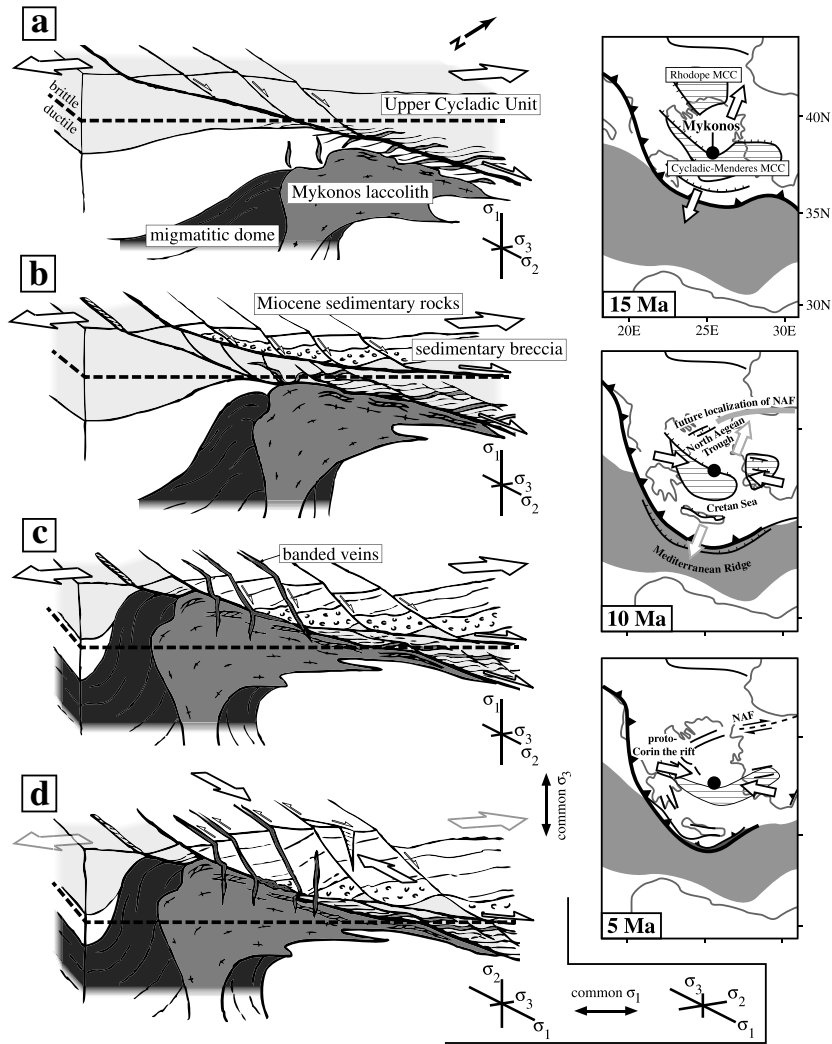


**Figure 15.** (a–d) 3-D views showing the structural evolution of Mykonos island during and after the activity of the detachments and the mineral deposition. The results of the successive stress regimes experienced by the region are also schematized (modified from Jolivet and Brun [2010]).

oriented N93°E and N191°E, respectively. It is noteworthy that the direction of the least principal stress axis is relatively similar to the one of the first normal faults system. Finally, the third faults system associated with E–W to NW–SE-trending reverse kinematic indicators consists in fault planes, sometimes the reworked detachment plane itself, with a wide range of orientation and a low dip. These structures are not compatible with the previous strike-slip and extensional stress regimes and another one is required. This third stress regime therefore shows a vertical  $\sigma_3$ , a  $\sigma_2$  with a N27°E direction and  $\sigma_1$  oriented N105°E close to the principal compressional stress axis of the strike-slip faults system.

[41] Integrating these data, we have isolated four to five main stages that characterized the tectonic evolution of Mykonos island.

[42] (1) The first ductile extensional stage is contemporaneous with the emplacement and cooling of the Mykonos laccolith as evidenced by the sub-solidus to post-solidus evolution of its deformation [Faure and Bonneau, 1988; Faure et al., 1991; Denèle et al., 2011] (Figure 15a). Consistent mineral and ductile fabric in the laccolith and in the

migmatitic dome indicates that exhumation of these two units occurs under a NE–SW extensional regime and a top-to-the-NE shearing (Figures 1b and 15a). At this stage, the Livada detachment, that affects the Upper Cycladic Unit, had a ductile behavior with the development of top-to-the-NE ductile shear bands (Figure 6).

[43] (2) Then, exhumation of the Mykonos laccolith brought this magmatic body in contact with the Livada detachment (Figure 15b) inducing a reactivation of the initial intrusive contact in ductile conditions. In the footwall, NE-shallow dipping foliation with a top-to-the-NE stretching lineation and mylonitic to ultramylonitic shear bands developed therefore within the laccolith, consistently with the top-to-the-NE extensional stress regime (Figures 6c and 6d). The Upper Cycladic Unit and intruding aplitic sills and dykes in the hanging wall of the Livada detachment were also affected by the top-to-the-NE ductile fabric (Figures 6a and 6b). Structurally, above the Mykonos detachment was initiated under brittle conditions contemporaneously with the deposition of late Miocene syn-rift sediments (Figure 15b). This sedimentary unit was

cut by NW–SE steep normal faults, defining a tilted-block geometry (Figures 3c, 7b, and 13a).

[44] (3) Then, the continuation of exhumation below the two branches of the NCDS of the Mykonos laccolith and the surrounding migmatitic dome was allowed for these two units to cross the ductile–brittle transition, some 11–10 Ma ago while the Livada detachment was reactivated under brittle conditions (Figure 15c). The Livada detachment is in place tectonically omitted due to intense normal faulting, and the cataclasites of the Mykonos detachment puts the late Miocene sediments in direct contact on top of the Mykonos laccolith (Figure 3). Contemporaneously, a series of sub-vertical banded veins develop during the activity of the detachments (Figures 9 and 15c). Hydrothermal fluids were thus mainly drained by tectonic structures like the NW–SE steep normal faults or the NCDS itself (Figure 4) where the mineralization can be striated with evidence of normal slip or brecciated (Figure 8d). Structural study of these brittle mineralized structures allows us to characterize this brittle extensional stage with a least principal stress ( $\sigma_3$ ) oriented  $\sim N40^\circ E$  (Figure 13b) that supports the formation of banded veins in NW–SE opening fractures (i.e., as tension gashes).

[45] (4) Then, a strike-slip stress regime developed, characterized by a permutation of  $\sigma_1$  and  $\sigma_2$ , whereas  $\sigma_3$  kept a consistent N–S to NE–SW orientation (Figure 13b). The NW–SE steep normal faults and veins were thus reactivated as left-lateral strike-slip faults, and some ENE–WSW right-lateral conjugate ones formed (Figures 11 and 15d). Detachment planes were thus dissected by these strike-slip structures as in Pano Tigani area (Figure 12). Some of these strike-slip veins were reactivated as normal faults, suggesting an alternation of stress regime during a transition phase while the mineralization continued to emplace (Figure 11a). Considering that the mineral deposition is a short-lived event, this transition phase may occur quickly after 11–10 Ma.

[46] (5) Finally, a switch of  $\sigma_2$  and  $\sigma_3$  could induce a compressional regime with a  $\sigma_1$  orientation close to  $N105^\circ E$  and NE–SW least horizontal stress direction ( $\sigma_2$ ) (Figures 13b and 15b). This stage would postdate the mineralization deposition and is characterized by newly formed small-scale reverse faults (Figure 11b) and by a slight local reactivation of the detachment planes with a reverse movement that can cut older strike-slip veins (Figure 12e). All of these structures show striae oriented  $\sim N110^\circ E$ .

[47] The succession of these different stages first suggests an evolution of a top-to-the-NE extensional deformation from ductile-to-brittle conditions. Then, a fast evolution of the brittle stress regime occurred during the emplacement of veins, 11–10 Ma ago, from a purely NE–SW extensional regime to a strike-slip and, finally, a possible late compressional one with the progressive development of an E–W to NW–SE compression and the persistence of an NE–SW least horizontal principal stress (Figure 13b). This orientation shows however a minor counterclockwise rotation of  $10\text{--}15^\circ$  between the extensional and the possible compressional stage that can be related to the rigid clockwise rotation of the Mykonos laccolith during its final cooling [Morris and Anderson, 1996; Avigad et al., 1998; Lecomte et al., 2010; Denèle et al., 2011].

[48] The finite strain amount is likely drastically different for each tectonic regime. The first stage is an extensional

stage consistent with the Aegean post-orogenic extension, therefore lasted some 25 My at regional scale. It mostly corresponds to several tens of kilometers of slip along the NCDS while the strike-slip stage corresponds to decametric to metric offsets of the detachment and reworking of the normal faults and associated veins. The possible final compressional stage is only associated to striae on the detachment plane and small-scale reverse faults, and no significant offset is observed. The stress regime has thus changed, but the overall structure has not been significantly modified (Figures 13a and 15d). However, this fast and subtle tectonic evolution, occurring at least partially during the mineralization deposition, is essential regarding the late Cenozoic geodynamics of the Aegean region.

#### 6.4. Implication of the Stress Regime Changes for Late Cenozoic Geodynamic Evolution of the Aegean Domain

[49] Evidence for a late E–W shortening has already been described elsewhere within the Cyclades and also farther to the east, in western Turkey [Angelier, 1976; Buick, 1991a,b; Bozkurt and Park, 1997; Ring et al., 1999; Avigad et al., 2001; Bozkurt, 2003]. Based on the existence of fold axes of various scales parallel to the stretching direction in the central and northern Cyclades, Buick [1991a; 1991b] and Avigad et al. [2001] proposed that the NE–SW extension that has prevailed in the Aegean since the late Oligocene was associated with a component of E–W shortening. Avigad et al. [2001] even concluded that during this period, the Aegean crust did not undergo significant thinning due to the combined effects of NE–SW stretching and E–W shortening. Some of these folds can be interpreted differently, as “a-type” folds parallel to the transport direction [Jolivet et al., 2004]. However, the late folding of the detachment, seen in Naxos, for instance [Avigad et al., 2001], and also the folding of mylonitic foliation in the Menderes massif [Bozkurt and Park, 1997], rather suggest a recent component of E–W shortening. Moreover, on the island of Samos in the eastern part of the Aegean Sea and also in the Menderes massif, the deformation of the Miocene–Pliocene sedimentary basins is notably characterized by a short E–W compressional event accompanied by a significant uplift [Angelier, 1976; Ring et al., 1999; Bozkurt, 2003]. The age of this event settled at 9–8.6 Ma [Weidmann et al., 1984; Ring et al., 1999], that is compatible with our estimation of the timing of the stress regime change on Mykonos island (Figure 14). Thus, although these features indicating a late compressional regime are not well expressed on Mykonos, the presence of contemporaneous compressional structures elsewhere in the region leads us to correlate the reworking of the Mykonos detachment and the development of small-scale reverse faults as a result of this late compressional event.

[50] The question then is the cause of this E–W shortening.

[51] One may argue, as Sengör and Bozkurt [2013], that such minor compressional structures could be part of the overall extensional activity of the detachment, but in the case of Mykonos, the compressional features clearly post-date both extensional and strike-slip structures.

[52] One other aspect to consider is the role of the gravitational forces [Molnar and Lyon-Caen, 1988; Vanderhaeghe, 2012]. Indeed, in their analog experiments, Gautier et al. [1999] show that transverse shortening during horizontal spreading of a thick continental lithosphere may develop as a

result of pure gravity spreading, associated with a pattern of faults and rotations. However, the stress regime change on Mykonos island occurred during the deposition of Mykonos mineralization in the early Tortonian (i.e., 11–10 Ma ago) at the earliest (Figure 14). This age is late compared to the timing of the post-orogenic extension in the Aegean domain that started some 35 Ma ago [Jolivet and Faccenna, 2000] indicating that the crust was already thinned in the early Tortonian. Therefore, body forces were probably insufficient to explain such stress regime evolution by itself.

[53] Another hypothesis to consider is the influence of exhumation processes on the evolution of stress regime. Indeed, in an extensional context, rock exhumation and crustal thinning are associated with a diminution of the vertical  $\sigma_1$ . If this trend continues, a switch of  $\sigma_1$  and  $\sigma_2$  can occur and therefore a strike-slip faults system can develop under brittle conditions. However, this process cannot explain the relatively important offset of the detachment due to the strike-slip stage as well as the late compressional event. Other causes for this evolution of the stress regime have to be considered.

[54] Nowadays, a component of E–W shortening is present in the deformation of the northern Aegean as shown by the GPS data [Le Pichon and Kreemer, 2010]. It is due to the westward motion of Anatolia along the North Anatolian Fault. If the NAF has reached the northern Aegean (Dardanelles Strait) some 6 Ma ago as a localized discontinuity [Armijo et al., 1999; Melinte-Dobrinescu et al., 2009], Şengör et al. [2005] proposed that the dextral shear has been active in northern Anatolia since some 13–11 Ma, a timing compatible with our observations on Mykonos (Figures 14 and 15) and also with the late folding of the detachment in Naxos [Avigad et al., 2001] and the ~9 Ma E–W compressional event in Samos [Ring et al., 1999]. Faccenna et al. [2006] further proposed that the westward motion of Anatolia was triggered, at least partly, by a slab detachment event below eastern Turkey, an event that can be related to a surge of volcanism in this region some 10 Ma ago [Şengör et al., 2008; Pearce et al., 1990]. Here also, the timing of this event is compatible with the late compressional deformation recorded on Mykonos.

## 7. Conclusion

[55] Our field observations show that mineralization on Mykonos island mainly corresponds to sub-vertical NW–SE extensional veins, developed essentially during the activity of the Livada and Mykonos detachments some 11–10 Ma ago. The veins emplaced shortly after the crossing of the ductile-brittle transition and up to shallow crustal levels during the latest cooling increments of the Mykonos laccolith. This hydrothermal mineralization then shows a clear temporal and kinematics relation with the NE–SW Aegean extensional dynamics.

[56] Finally, this study leads to highlight a change of stress directions during the deposition of the mineralization. Indeed, from purely extensional, the stress regime becomes progressively more compressional with the development of strike-slip faults reactivating some of the veins and even small-scale reverse faults. During this period, the least horizontal stress was consistently oriented NE–SW. The increase of the E–W compressional component from 11–10 Ma ago is probably a consequence of the inception of the

westward motion of Anatolia some 4 Ma before the propagation of the NAF in the Aegean domain and the localization of extension on the Aegean Sea margins.

[57] **Acknowledgments.** The authors wish to express their thanks to Olivier Vanderhaeghe, Erdin Bozkurt, and an anonymous reviewer for their constructive comments.

[58] This study was funded by the Institut Universitaire de France and partly by the ERC Advanced Research Grant RHEOLITH.

## References

- Altherr, R., H. Kreuzer, I. Wendt, H. Lenz, G. A. Wagner, J. Keller, W. Harre, and A. Hohndorf (1982), A Late Oligocene/Early Miocene high temperature belt in the anti-cycladic crystalline complex (SE Pelagonian, Greece), *Geol. Jb.*, *23*, 97–164.
- Altherr, R., and W. Siebel (2002), I-type plutonism in a continental back-arc setting: Miocene granitoids and monzonites from the central Aegean Sea, Greece, *Contrib. Mineral. Petrol.*, *143*, 397–415.
- Angelier, J. (1976), Sur l'alternance moi-plio-quaternaire de mouvements extensifs et compressifs en Égée orientale: l'île de Samos (Grèce), *C. R. Acad. Sci. Paris*, *283*, 463–466.
- Angelier, J. (1979), Determination of the mean principal directions of stress for a given fault population, *Tectonophysics*, *56*, 17–26.
- Angelier, J. (1994), Paleostress determinations, in *Continental Deformations*, edited by P. L. Hancock, Pergamon Press, Tarrytown, N.Y., 53–100.
- Armijo, R., B. Meyer, G. C. P. King, A. Rigo, and D. Papanastassiou (1996), Quaternary evolution of the Corinth Rift and its implications for the Late Cenozoic evolution of the Aegean, *Int. J. Geophys.*, *126*, 11–53.
- Armijo, R., B. Meyer, A. Hubert, and A. Barka (1999), Westward propagation of the north Anatolian into the northern Aegean: Timing and kinematics, *Geology*, *27*(3), 267–270.
- Avigad, D., G. Baer, and A. Heimann (1998), Block rotations and continental extension in the central Aegean Sea: palaeomagnetic and structural evidence from Tinos and Mykonos, *Earth Planet. Sci. Lett.*, *157*, 23–40.
- Avigad, D., A. Ziv, and Z. Garfunkel (2001), Ductile and brittle shortening, extension-parallel folds and maintenance of crustal thickness in the Central Aegean, *Tectonics*, *20*(2), 277–287.
- Bonneau, M., and J. R. Kienast (1982), Subduction, collision et schistes bleus: Exemple de l'Égée, Grèce, *Bull. Soc. géol. France*, *7*, 785–791.
- Bozkurt, E., and R. G. Park (1997), Evolution of a mid-Tertiary extensional shear zone in the Southern Menderes Massif, western Turkey, *Bull. Soc. géol. France*, *168*, 3–14.
- Bozkurt, E. (2003), Origin of NE-trending basins in Western Turkey, *Geodinamica Acta*, *16*, 61–81.
- Brichau, S., U. Ring, R. A. Ketcham, A. Carter, D. Stockli, and M. Brunel (2006), Constraining the long-term evolution of the slip rate for a major extensional fault system in the central Aegean, Greece, using thermochronology, *Earth Planet. Sci. Lett.*, *241*, 293–306.
- Brichau, S., U. Ring, A. Carter, P. Monie, R. Bolhar, D. Stockli, and M. Brunel (2007), Extensional faulting on Tinos Island, Aegean Sea, Greece: How many detachments?, *Tectonics*, *26*, TC4009, doi:10.1029/2006TC001969.
- Brichau, S., U. Ring, A. Carter, R. Bolhar, P. Monié, D. Stockli, and M. Brunel (2008), Timing, slip rate, displacement and cooling history of the Mykonos detachment footwall, Cyclades, Greece, and implications for the opening of the Aegean Sea basin, *J. Geol. Soc. London*, *165*, 263–277.
- Brichau, S., S. Thomson, and U. Ring (2010), Thermochronometric constraints on the tectonic evolution of the Serifos detachment, Aegean Sea, Greece, *Int. J. Earth Sci. (Geol. Rundsch)*, *99*, 379–393, doi:10.1007/s00531-00008-00386-00530.
- Brun, J. P., and C. Faccenna (2008), Exhumation of high-pressure rocks driven by slab rollback, *Earth Planet. Sci. Lett.*, *272*, 1–7, doi:10.1016/j.epsl.2008.1002.1038.
- Buick, I. S. (1991a), Mylonite fabric development on Naxos, Greece, *J. Struct. Geol.*, *13*(6), 643–655.
- Buick, I. S. (1991b), The late Alpine evolution of an extensional shear zone, Naxos, Greece, *J. Geol. Soc. London*, *148*, 93–103.
- Cathelineau, M., and D. Nieva (1985), A chlorite solid solution geothermometer. The Los Azufres (Mexico) geothermal system, *Contrib. Mineral. Petrol.*, *91*, 235–244.
- Cathelineau, M. (1988), Cation site occupancy in chlorites and illites as a function of temperature, *Clay Miner.*, *23*, 471–485.
- de Boorder, H., W. Spakman, S. H. White, and M. J. R. Wortel (1998), Late Cenozoic mineralization, orogenic collapse and slab detachment in the European Alpine Belt, *Earth Planet. Sci. Lett.*, *164*, 569–575.
- Denèle, Y., E. Lecomte, L. Jolivet, O. Lacombe, L. Labrousse, B. Huet, and L. Le Pourhiet (2011), Granite intrusion in a metamorphic core complex:

- The example of the Mykonos laccolith (Cyclades, Greece), *Tectonophysics*, 501, 52–70, doi:10.1016/j.tecto.2011.1001.1013.
- Dercourt, J., et al. (1986), Geological evolution of the Tethys belt from the Atlantic to the Pamir since the Lias, *Tectonophysics*, 123, 241–315.
- Dercourt, J., L. E. Ricou, and B. Vrielinck. (1993), *Atlas Tethys Palaeo-environmental maps*, 307 p., Gauthier-Villars, Paris.
- Duchêne, S., R. Aïssa, and O. Vanderhaeghe (2006), Pressure-temperature-time evolution of metamorphic rocks from Naxos (Cyclades, Greece): Constraints from thermobarometry and Rb/Sr dating, *Geodinamica Acta*, 19(5), 299–319.
- Faccenna, C., O. Bellier, J. Martinod, C. Piromallo, and V. Regard (2006), Slab detachment beneath eastern Anatolia: A possible cause for the formation of the North Anatolian fault, *Earth Planet. Sci. Lett.*, 242, 85–97.
- Faure, M., and M. Bonneau (1988), Données nouvelles sur l'extension néogène de l'Égée: La déformation ductile du granite miocène de Mykonos (Cyclades, Grèce), *C. R. Acad. Sci. Paris*, 307, 1553–1559.
- Faure, M., M. Bonneau, and J. Pons (1991), Ductile deformation and syntectonic granite emplacement during the late Miocene extension of the Aegean (Greece), *Bull. Soc. géol. France*, 162, 3–12.
- Gautier, P., and J. P. Brun (1994a), Crustal-scale geometry and kinematics of late-orogenic extension in the central Aegean (Cyclades and Evvia island), *Tectonophysics*, 238, 399–424.
- Gautier, P., and J. P. Brun (1994b), Ductile crust exhumation and extensional detachments in the central Aegean (Cyclades and Evvia islands), *Geodinamica Acta*, 7(2), 57–85.
- Gautier, P., J. P. Brun, R. Moriceau, D. Sokoutis, J. Martinod, and L. Jolivet (1999), Timing, kinematics and cause of Aegean extension: A scenario based on a comparison with simple analogue experiments, *Tectonophysics*, 315, 31–72.
- Govers, R., and M. J. R. Wortel (2005), Lithosphere tearing at STEP faults: Response to edges of subduction zones, *Earth Planet. Sci. Lett.*, 236 505–523.
- Grasemann, B., D. A. Schneider, D. F. Stockli, and C. Iglšeder (2012), Miocene bivertgent crustal extension in the Aegean: Evidence from the western Cyclades (Greece), *Lithosphere*, doi:10.1130/L1164.1131.
- Huet, B., L. Labrousse, and L. Jolivet (2009), Thrust or detachment? Exhumation processes in the Aegean: Insight from a field study on Ios (Cyclades, Greece), *Tectonics*, 28, TC3007, doi:10.1029/2008TC002397.
- Jiang, W.-T., D. R. Peacor, and P. R. Buseck (1994), Chlorite geothermometry?—Contamination and apparent octahedral vacancies, *Clays Clay Miner.*, 42(5), 593–605.
- Jolivet, L., J. P. Brun, P. Gautier, S. Lallemand, and M. Patriat (1994), 3-D kinematics of extension in the Aegean from the Early Miocene to the Present, insight from the ductile crust, *Bull. Soc. géol. France*, 165, 195–209.
- Jolivet, L., and M. Patriat (1999), Ductile extension and the formation of the Aegean Sea, in *The Mediterranean Basins: Tertiary Extension within the Alpine Orogen*, edited by B. Durand, L. Jolivet, F. Horváth, and M. Séranne, 156, 427–456, Spe. Pub. – Geol. Soc. London.
- Jolivet, L., and C. Faccenna (2000), Mediterranean extension and the Africa-Eurasia collision, *Tectonics*, 19(6), 1095–1106.
- Jolivet, L. (2001), A comparison of geodetic and finite strain pattern in the Aegean, geodynamic implications, *Earth Planet. Sci. Lett.*, 5793, 1–10.
- Jolivet, L., C. Faccenna, B. Goffé, E. Burov, and P. Agard (2003), Subduction tectonics and exhumation of high-pressure metamorphic rocks in the Mediterranean orogens, *Am. J. Sci.*, 303, 353–409.
- Jolivet, L., V. Famin, C. Mehl, T. Parra, C. Aubourg, R. Hébert, and P. Philippot (2004), Strain localization during crustal-scale boudinage to form extensional metamorphic domes in the Aegean Sea, *Spe. Pap. – Geol. Soc. Am.*, 380, 185–210.
- Jolivet, L., and J. P. Brun (2010), Cenozoic geodynamic evolution of the Aegean region, *Int. J. Earth Sci.*, 99, 109–138, doi:10.1007/s00531-00008-00366-00534.
- Jolivet, L., E. Lecomte, B. Huet, Y. Denèle, O. Lacombe, L. Labrousse, L. Le Pourhiet, and C. Mehl (2010), The north cycladic detachment system, *Earth Planet. Sci. Lett.*, 289, 87–104, doi:10.1016/j.epsl.2009.1010.1032.
- Keiter, M., K. Piepjohn, C. Ballhaus, M. Lagos, and M. Bode (2004), Structural development of high-pressure metamorphic rocks on Syros island (Cyclades, Greece), *J. Struct. Geol.*, 26, 1433–1445.
- Kranidiotis, P., and W. H. MacLean (1987), Systematics of chlorite alteration at the Phelps Dodge massive sulfide deposit, Matagami, Quebec, *Econ. Geol.*, 82(7), 1898–1911, doi:10.2113/gsecongeo.82.7.1898.
- Kumerics, C., U. Ring, S. Brichau, J. Glodny, and P. Monié (2005), The extensional Messaria shear zone and associated brittle detachment faults, Aegean Sea, Greece, *J. Geol. Soc.*, 162(4), 701–721.
- Le Pichon, X., and J. Angelier (1979), The Hellenic arc and trench system: A key to the neotectonic evolution of the eastern Mediterranean area, *Tectonophysics*, 60, 1–42.
- Le Pichon, X., and C. Kreemer (2010), The Miocene-to-present kinematic evolution of the Eastern Mediterranean and Middle East and its implications for dynamics, *Annu. Rev. Earth Planet. Sci.*, 38, 323–351, doi:10.1146/annurev-earth-040809-152419.
- Lecomte, E., L. Jolivet, O. Lacombe, Y. Denèle, L. Labrousse, and L. Le Pourhiet (2010), Geometry and kinematics of a low-angle normal fault on Mykonos island (Cyclades, Greece): Evidence for slip at shallow dip, *Tectonics*, 29, TC5012, doi:10.1029/2009TC002564.
- Lecomte, E., L. Le Pourhiet, O. Lacombe, and L. Jolivet (2011), A continuum mechanics approach to quantify brittle strain on weak faults: application to the extensional reactivation of shallow dipping discontinuities, *Int. J. Geophys.*, 184, 1–11.
- Lee, J., and G. S. Lister (1992), Late Miocene ductile extension and detachment faulting, Mykonos, Greece, *Geology*, 20, 121–124.
- Lister, G. S., G. Banga, and A. Feenstra (1984), Metamorphic core complexes of cordilleran type in the Cyclades, Aegean Sea, Greece, *Geology*, 12, 221–225.
- Lucas, I. (1999), *Le pluton de Mykonos-Delos-Rhenee (Cyclades, Grèce): Un exemple de mise en place synchrone de l'extension crustale*, 491 pp, Université d'Orléans, Orléans.
- Martin, L., S. Duchêne, E. Delouie, and O. Vanderhaeghe (2006), The isotopic composition of zircon and garnet: A record of the metamorphic history of Naxos, Greece, *Lithos*, 87, 174–192.
- Mehl, C., L. Jolivet, and O. Lacombe (2005), From ductile to brittle: evolution and localization of deformation below a crustal detachment (Tinos, Cyclades, Greece), *Tectonics*, 24, TC4017, doi:10.1029/2004TC001767.
- Melinte-Dobrinescu, M. C., et al. (2009), The Messinian salinity crisis in the Dardanelles region: Chronostratigraphic constraints, *Palaeogeogr. Palaeoclimatol. Palaeoecol.*, 278, 24–39, doi:10.1016/j.palaeo.2009.1004.1009.
- Molnar, P., and H. Lyon-Caen (1988), Some simple physical aspects of the support, structure, and evolution of mountain belts, *Spe. Pap. – Geol. Soc. Am.*, 218, 179–207.
- Morris, A., and M. Anderson (1996), First paleomagnetic results from the Cycladic Massif, Greece, and their implications for Miocene extension directions and tectonic models in the Aegean, *Earth Planet. Sci. Lett.*, 142, 397–408.
- Pearce, J. A., J. F. Bender, S. E. Delong, W. S. F. Kidd, P. J. Low, Y. Guner, F. Saroglu, Y. Yilmaz, S. Moorbath, and J. G. Mitchell (1990), Genesis of collision volcanism in eastern Anatolia, Turkey, *J. Volcanol. Geotherm. Res.*, 44, 189–229.
- Pe-Piper, G., and D. J. W. Piper (2002), The igneous rocks of Greece. The anatomy of an orogen, 573 pp., Gebrüder Borntraeger, Berlin-Stuttgart.
- Pe-Piper, G., and D. J. W. Piper (2006), Unique features of the Cenozoic igneous rocks of Greece, in *Postcollisional Tectonics and Magmatism in the Mediterranean Region and Asia*, edited by Y. Dilek and S. Pavlides, pp. 259–282, doi:10.1130/2006.2409(1114), Geol. Soc. of Am., Boulder, Colo.
- Philippon, M., J. P. Brun, and F. Gueydan (2011), Tectonics of Syros Island Blueschists (Cyclades, Greece): From subduction to Aegean extension, *Tectonics*, 30, TC4001, doi:10.1029/2010TC002810.
- Reilinger, R. E., S. C. McClusky, M. B. Oral, R. W. King, M. N. Tokoz, A. A. Barka, I. Kinik, O. Lenk, and I. Sanli (1997), Global positioning system measurements of present-day crustal movements in the Arabia-Africa-Eurasia plate collision zone, *J. Geophys. Res.*, 102, 9983–9999.
- Reilinger, R., S. McClusky, D. Paradissis, S. Ergintav, and P. Vernant (2010), Geodetic constraints on the tectonic evolution of the Aegean region and strain accumulation along the Hellenic subduction zone, *Tectonophysics*, 488, 22–30.
- Reynolds, S. J., and G. S. Lister (1987), Structural aspects of fluid-rock interactions in detachment zones, *Geology*, 15, 362–366.
- Ring, U., S. Laws, and M. Bernet (1999), Structural analysis of a complex nappe sequence and late-orogenic basins from the Aegean Island of Samos, Greece, *J. Struct. Geol.*, 21, 1575–1601.
- Ring, U., and P. W. Layer (2003), High-pressure metamorphism in the Aegean, eastern Mediterranean: Underplating and exhumation from the Late Cretaceous until the Miocene to recent above the retreating Hellenic subduction zone, *Tectonics*, 22(3), 1022, doi:10.1029/2001TC001350.
- Ring, U., T. Will, J. Glodny, C. Kumerics, K. Gessner, S. Thomson, T. Güngör, P. Monie, M. Okrusch, and K. Drüppel (2007), Early exhumation of high-pressure rocks in extrusion wedges: Cycladic blueschist unit in the eastern Aegean, Greece, and Turkey, *Tectonics*, 26, TC2001, doi:10.1029/2005TC001872.
- Ring, U., J. Glodny, T. Will, and S. Thomson (2010), The Hellenic subduction system: High-pressure metamorphism, exhumation, normal faulting, and large-scale extension, *Annu. Rev. Earth Planet. Sci.*, 38, 45–76, doi:10.1146/annurev-earth.050708.170910.
- Royden, L. H., and D. J. Papanikolaou (2011), Slab segmentation and late Cenozoic disruption of the Hellenic arc, *Geochem. Geophys. Geosyst.*, 12, Q03010, doi:10.1029/2010GC003280.
- Sánchez-Gómez, M., D. Avigad, and A. Heiman (2002), Geochronology of clasts in allochthonous Miocene sedimentary sequences on Mykonos and

- Paros islands: Implications for back-arc extension in the Aegean Sea, *J. Geol. Soc. London*, 159, 45–60.
- Sengör, A. M. C., O. Tüysüz, C. Imren, M. Sakiç, H. Eyidogan, N. Görür, X. Le Pichon, and C. Rangin (2005), The North Anatolian fault: A new look, *Annu. Rev. Earth Planet. Sci.*, 33, 37–112, doi:10.1146/annurev.earth.32.101802.120415.
- Sengör, A. M. C., M. S. Özeren, M. Keskin, M. Sakiç, A. D. Özbakir, and I. Kayan (2008), Eastern Turkish high plateau as a small Turcic-type orogen: Implications for post-collisional crust-forming processes in Turcic-type orogens, *Earth-Sci. Rev.*, 90, 1–48.
- Sengör, A. M. C., and E. Bozkurt (2013), Layer-parallel shortening and related structures in zones undergoing active regional horizontal extension, *Int. J. Earth Sci.*, 102, 101–119.
- Skarpelis, N. (2002), Geodynamics and evolution of the Miocene mineralization in the Cycladic-Pelagion belt, Hellenides, *Bull. Geol. Soc. Greece*, XXXIV(6), 2191–2206.
- Skarpelis, N., and H. A. Gilg (2006), Miocene extensional fault-controlled mineralization in the central Aegean (Mykonos, Cyclades): Deposition from a two-stage hydrothermal system?, *NECAM 2006*, International Conference, Milos.
- Stampfli, G. M. (2000), Tethyan oceans, *Spec. Pub. - Geol. Soc. London*, 173, 1–23.
- Stöckhert, B., M. R. Brix, R. Kleinschrodt, A. J. Hurford, and R. Wirth (1999), Thermochronometry and microstructures of quartz—a comparison with experimental flow laws and predictions on the temperature of the brittle-plastic transition, *J. Struct. Geol.*, 21(3), 351–369.
- Stouraiti, C., P. Mitropoulos, J. Tarney, B. Barreiro, A. M. McGrath, and E. Baltatzis (2010), Geochemistry and petrogenesis of late Miocene granitoids, Cyclades, southern Aegean: Nature of source components, *Lithos*, 114, 337–352, doi:10.1016/j.lithos.2009.09.010.
- Trotet, F., L. Jolivet, and O. Vidal (2001), Tectono-metamorphic evolution of Syros and Sifnos islands (Cyclades, Greece), *Tectonophysics*, 338, 179–206.
- Vanderhaeghe, O. (2004), Structural development of the Naxos migmatite dome, *Spe. Pap. - Geol. Soc. Am.*, 380, 211–227.
- Vanderhaeghe, O. (2012), The thermal-mechanical evolution of crustal orogenic belts at convergent plate boundaries: A reappraisal of the orogenic cycle, *J. Geodyn.*, 56–57, 124–145.
- van Hinsbergen, D. J. J., W. J. Zachariasse, M. J. R. Wortel, and J. E. Meulenkamp (2005), Underthrusting and exhumation: A comparison between the external Hellenides and the “hot” Cycladic and “cold” South Aegean core complexes (Greece), *Tectonics*, 24, TC2011, doi:10.1029/2004TC001692.
- Vidal, O., T. Parra, and F. Trotet (2001), A thermodynamic model for Fe-Mg aluminous chlorite using data from phase equilibrium experiments and natural pelitic assemblages in the 100° to 600°C, 1 to 25 kb range, *Am. J. Sci.*, 301, 557–592.
- Walcott, C. R., and S. H. White (1998), Constraints on the kinematics of post-orogenic extension imposed by stretching lineations in the Aegean region, *Tectonophysics*, 298, 155–175.
- Walshe, J. L. (1986), A six-component chlorite solid solution model and the conditions of chlorite formation in hydrothermal and geothermal systems, *Econ. Geol.*, 81(3), 681–703, doi:10.2113/gsecongeo.81.3.681.
- Weidmann, M., N. Solounias, R. E. Drake, and G. H. Curtis (1984), Neogene stratigraphy of the eastern basin, Samos island, Greece, *Geobios*, 17(4), 477–490.
- Wijbrans, J. R., and I. McDougall (1986), <sup>40</sup>Ar/<sup>39</sup>Ar dating of white micas from an alpine high-pressure metamorphic belt on Naxos (Greece): the resetting of the argon isotopic system, *Contrib. Mineral. Petrol.*, 93, 187–194.
- Wijbrans, J. R., and I. McDougall (1988), Metamorphic evolution of the Attic Cycladic metamorphic belt on Naxos (Cyclades, Greece) utilizing <sup>40</sup>Ar/<sup>39</sup>Ar age spectrum measurements, *J. Metamorph. Geol.*, 6, 571–594.
- Žalohar, J., and M. Vrabec (2007), Paleostress analysis of heterogeneous fault-slip data: The Gauss method, *J. Struct. Geol.*, 29, 1798–1810.